ACS Biomaterials SCIENCE & ENGINEERING
Cite This: ACS Biomater. Sci. Eng. XXXX, XXX, XXX−XXX
Article
pubs.acs.org/journal/abseba

Investigating the Role of Sustained Calcium Release in Silk-Gelatin-Based Three-Dimensional Bioprinted Constructs for Enhancing the Osteogenic Differentiation of Human Bone Marrow Derived Mesenchymal Stromal Cells

Aarushi Sharma,[†] Giovanna Desando,[‡] Mauro Petretta,[‡,§] Shikha Chawla,[†] Isabella Bartolotti,[‡] Cristina Manferdini,[∥] Francesca Paolella,[∥] Elena Gabusi,[∥] Diego Trucco,[∥] Sourabh Ghosh,*[,†] and Gina Lisignoli*[,∥]

[†]Regenerative Engineering Laboratory, Department of Textile Technology, Indian Institute of Technology, New Delhi 110016, India
[‡]IRCCS Istituto Ortopedico Rizzoli, Laboratorio RAMSES, Bologna 40136, Italy
[§]RegenHu Ltd, Villaz St. Pierre CH-1690, Switzerland
[∥]Laboratorio di Immunoreumatologia e Rigenerazione Tissutale, IRCCS Istituto Ortopedico Rizzoli, Bologna 40136, Italy

Supporting Information

ABSTRACT: Scaffold-based bone tissue engineering strategies fail to meet the clinical need to fabricate patient-specific and defect shape-specific, anatomically relevant load-bearing bone constructs. 3D bioprinting strategies are gaining major interest as a potential alternative, but design of a specific bioink is still a major challenge that can modulate key signaling pathways to induce osteogenic differentiation of progenitor cells, as well as offer appropriate microenvironment to augment mineralization. In the present study, we developed silk fibroin protein and gelatin-based conjugated bioink, which showed localized presence and sustained release of calcium. Presence of 2.6 mM Ca^{2+} ions within the bioink could further induce enhanced osteogenesis of Bone marrow derived progenitor cells (hMSCs) compared to the bioink without calcium, or same concentration of calcium added to the media, as evidenced by upregulated gene expression of osteogenic markers. This study generated unprecedented mechanistic insights on the role of fibroin-gelatin-$CaCl_2$ bioink in modulating expression of several proteins which are known to play crucial role in bone regeneration as well as key signaling pathways such as β-catenin, BMP signaling pathway, Parathyroid hormone-dependent signaling pathway, Forkhead box O (FOXO) pathway, and Hippo pathways in hMSC-laden bioprinted constructs.

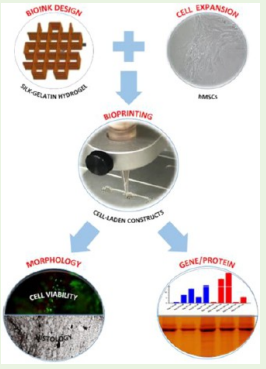

KEYWORDS: *silk bioink, osteogenesis, 3D bioprinting, extracellular calcium, signaling pathways*

INTRODUCTION

Bones are developed and continuously remodelled by a series of complex events of mineralization performed by osteoblasts and resorption performed by osteoclasts, following a variety of metabolic, physical, and endocrine stimuli.[1] Three-dimensional (3D) bioprinting is a promising strategy to develop osteoinductive and osteoconductive "smart" biomaterials mimicking the bone tissue specific extracellular matrix (ECM), to recapitulate an appropriate bone architecture and to ensure key physiological functions of the osteoprogenitor cells.[2] Designed biomaterials-based bioinks and the use of 3D bioprinting technology can offer new perspectives for developing defect site-specific and patient-specific bone constructs.

Various biomaterials, spanning from natural to synthetic hydrogels, have already been investigated to promote bone regeneration.[1] Silk fibroin has emerged as a potential bone regeneration biomaterial[2] because of its several chemical and biological properties.[3] Silk can be used in various architectural forms, such as hydrogels,[4] salt leached porous scaffolds,[5] textile braids,[6] 3D printed direct-write scaffolds,[7] and composites.[8] Native silk fibers have high mechanical properties due to high β-sheet content and orientation,[9] offer satisfactory cytocompatibility[10] and minimal immunogenic response.[11] Mineralization of *Bombyx mori* native silk fiber-based textile braids resulted in preferential growth of needle-like hydroxyapatite nanocrystals along the *c*-axis, recapitulating mineralization process on collagen type I (COL I) in human bone, and achieved Ca/P ratio comparable to commercial hydroxyapatite.[9] As the entire amino acid sequence for *Bombyx mori* silk fibroin is known, it can be chemically modified (such as carbodimide chemistry and diazonium coupling[5]) and functionalized with specific bioactive osteogenic motifs to activate specific cellular signaling pathway. To this end, first

Received: December 25, 2018
Accepted: February 12, 2019
Published: February 12, 2019

DOI: 10.1021/acsbiomaterials.8b01631
ACS Biomater. Sci. Eng. XXXX, XXX, XXX−XXX

attempts from our group were focused on elucidation of role of silk-gelatin (SF-G) bioink, in the presence of triiodothyronine hormone in media, to induce endochondral ossification by activation of the Wnt/β-catenin, Indian hedgehog, and parathyroid hormone (PTH) signaling pathways.[12]

It is well-known that the maintenance of bone homeostasis is guaranteed by the extracellular free calcium (Ca^{2+}) released by osteoclasts from the mineralized bone matrix into the extracellular fluid[13] during bone resorption. Therefore, the response of osteoprogenitors to Ca^{2+} present in extracellular microenvironment is of prime concern for normal bone remodelling and it has to be considered for bone tissue engineering approaches.[14] It is also known that a sustained dosage of Ca^{2+} can drastically modulate the in vitro signaling networks akin to their in vivo counterparts.[15−17] On the basis of these biological considerations, ceramic scaffolds are among the most commonly used materials for bone regeneration, because of the similar chemical composition of these materials to the inorganic mineral phase of the bone[18−20] and their ability to degrade and release Ca^{2+}.[21] However, the ceramic scaffolds are highly brittle and are thus unsuitable to develop custom-made patient-specific constructs.[18] We previously demonstrated the osteogenic potential of extracellular calcium ions on osteoblasts in monolayer culture.[17] Osteoblasts cultured in media containing 2.6 mM Ca^{2+} demonstrated upregulated osteogenic differentiation as compared to osteoblasts cultured in media without Ca^{2+}.[17] Thus, in the current study, we functionalized 3D bioprinted SF-G bioinks with Ca^{2+} to improve the osteogenic potential of human bone marrow-derived mesenchymal stromal cells (hMSCs).

The three main objectives of the current study were aimed at (1) the optimization of rheological properties of the newly developed SF-G bioink functionalized with calcium to develop stable, self-supporting cytocompatible constructs; (2) the assessment of the osteogenic potential of SF-G bioink by adding Ca^{2+} (SF-G-$CaCl_2$) in the presence and absence of pro-osteogenic factors (OFs); (3) the identification of the signaling pathways regulating the osteogenic differentiation of hMSCs encapsulated in the 3D bioprinted SF-G constructs in the presence and absence of Ca^{2+}. We performed a series of histological, gene and mass spectrometry based-proteomics analysis to identify the biological signaling mechanisms involved in osteogenic differentiation of the 3D bioprinted SF-G under the effect of the sustained dosage of Ca^{2+}.

MATERIALS AND METHODS

SF-G Bioink Formulation (with and without $CaCl_2$). 5% w/v *Bombyx mori* silk fibroin (SF) solution was prepared as described in our previous studies.[22,23] Both 5% SF and 5% SF combined with four different concentrations of $CaCl_2$: 1.5, 2.6, 10, and 50 mM (5% SF-$CaCl_2$) were autoclaved, whereas 5% w/v of gelatin from porcine skin (Sigma−Aldrich, USA) was sterilized with 100% ethanol under laminar flow.[4] SF and SF-$CaCl_2$ were first combined with gelatin (G) and incubated for 30 min at 37 °C in order to obtain SF-G and SF-G-$CaCl_2$ blends, respectively. Then, these blends were separately mixed with 10× Dulbecco modified Eagle's (DMEM) medium with no calcium and high glucose (Gibco Life Technologies, USA) and 10% fetal bovine serum (FBS) (Euroclone S.p.a., Italy) for 15 min at 37 °C. After obtaining a homogeneous mixture of the SF-G and SF-G-$CaCl_2$ bioinks, 430 U of mushroom tyrosinase (Sigma−Aldrich, USA) was added at room temperature (RT) for cross-linking.

Rheological Characterization of SF-G-$CaCl_2$ Blends. The rheological properties of SF-G and SF-G-$CaCl_2$ blends were measured at 20 °C using plate and plate geometry of Anton Paar MCR-302. Four SF-G-$CaCl_2$ blend compositions (SF-G-1.5 mM $CaCl_2$, SF-G-2.6 mM $CaCl_2$, SF-G-10 mM $CaCl_2$, and SF-G-50 mM $CaCl_2$) were analyzed for characterization of rheological properties. The flow behavior was measured in the shear rate ranging from 0.1 to 1000 s^{-1} in rate-controlled mode by selecting 21 points in each decade. The flow behavior was further evaluated on the basis of power law equation for shear rate region of 1 to 100 s^{-1}. The equation was developed using the software ORIGIN 8.5 (Northampton, USA) for this region. The n-value has been calculated to evaluate the slope of the generated curves.

Further, the modulation of complex viscosity of the SF-G and all the SF-G-$CaCl_2$ blends was evaluated immediately after the addition of 430 U of tyrosinase (Sigma-Aldrich). Rheological characterizations were conducted with a cone−plate rheometer RheoStress 6000, Thermo Scientific) by two series of tests. The cone had a diameter of 35 mm and angle of 1 degree; the plate had a diameter of 60 mm. First, an amplitude sweep was performed with a constant frequency of 1 Hz and strain range from 0.1 to 100%. Then, the linear viscosity region was extrapolated from the viscosity trend as a strain function and the strain value of 1% was chosen for the following frequency sweep. In order to obtain the viscosity trend as a function of shear rate (s^{-1}), the frequency sweep was performed with a frequency range from 0.1 to 100 Hz. This test was conducted on SF-G blend for 72 min with steps of 12 min. During these steps, cross-linking of the SF-G and SF-G-$CaCl_2$ blend was induced using Tyrosinase enzyme. Based on the generated data, complex viscosity was estimated to have insight of the gelation behavior with respect to time, for a range of 0−3250 s. The range was considered equivalent to the time taken during printing of the bioink at a constant shear rate of 10 s^{-1}.

To assess the stability and sol−gel transition of the bioink post printing all the SF-G blends were processed to check the modulus in liquid phase. The dynamic elastic modulus (G') and viscous modulus (G'') were measured in oscillatory mode form 0.01 to 100% strain.

CAD Construct Design. The 10 layered 3D constructs were designed using BioCAD software (RegenHU, CH) with dimensions of 5 mm × 5 mm (length × width) and an interfilament distance of 1000 μm (Figure 2a, b). The layer height was set to 200 μm, and the deposition pattern was chosen to be 0/90°. The realized design was then converted into G-CODE instructions for the printing platform (3D Discovery, RegenHU, CH) and loaded in the Human Machine Interface (HMI) software (RegenHU, CH).

Ion Release Profile of Ca^{2+} Ions. SF-G-$CaCl_2$ (2.6 mM $CaCl_2$) 3D printed scaffolds were developed using the parameters described above. A needle with inner diameter of 200 μm was used, and the bioink-loaded cartridge was inserted into the printhead holder of the bioprinting platform and maintained at 22 ± 1 °C. The scaffolds were printed at the writing speed of 2 mm/s at 1 bar pressure. Ion release profile of Ca^{2+} ions from the SF-G-$CaCl_2$ scaffolds was monitored using inductively coupled plasma mass spectrometry (ICP-MS) (Agilent 7900 ICP-MS instrument). The SF-G-$CaCl_2$ 3D printed scaffolds were incubated in DMEM for the whole culture period and the supernatants were collected at the specific time points of days 1, 7, 14, and 21 and Ca^{2+} ion release was monitored. Data were normalized with respect to the DMEM and plotted using ORIGIN 8.

Preparation of Cell-Laden 3D Bioprinted Constructs. Two rounds of bioprinting processes were performed to obtain hMSC laden 5% SF-G and 5% SF-G-$CaCl_2$ constructs. Briefly, 5% SF-G and 5% SF-G-$CaCl_2$ were mixed with DMEM calcium-free, high glucose medium (Gibco) and 10% FBS (Euroclone), as well described above, in order to ensure a good cell viability. As for cell preparation, human bone marrow was harvested from an anonymous healthy donor, previously screened and selected from a pool of donors stored in our lab Biobank (at Istituto Ortopedico Rizzoli), to obtain hMSCs and, biological triplicates were carried out. Cell isolation was performed with standard procedures and then, cells were expanded and evaluated by FACS analysis for typical hematopoietic and nonhematopoietic markers, as already described in our previous work.[24] Ten ×10^6 hMSCs at passage 3 were mixed with 1.5 mL of SF-G and SF-G-$CaCl_2$ blends immediately after the addition of 430 U of tyrosinase (Sigma-Aldrich) under laminar flow at RT. hMSCs laden SF-G and SF-G-$CaCl_2$ bioinks were gently loaded onto sterile cartridges with a steel

DOI: 10.1021/acsbiomaterials.8b01631
ACS Biomater. Sci. Eng. XXXX, XXX, XXX−XXX

Table 1. Power Law Equation and Variables Found for the Bioinks

sample no.	sample ID	power law equation (η = viscosity; γ= shear rate)	R^2 value of equation	k = flow consistency index (Pa s^n)	n= power law index (dimensionless)
1	SF-G	$\eta = 0.1997\gamma^{-0.884}$	0.9957	0.1997	0.116
2	SF-G-1.5 mM $CaCl_2$	$\eta = 0.29\gamma^{-0.707}$	0.9915	0.29	0.123
3	SF-G-2.6 mM $CaCl_2$	$\eta = 0.23\ \gamma^{-0.949}$	0.9989	110.98	0.051
4	SF-G-10 mM $CaCl_2$	$\eta = 0.357\ \gamma^{-0.982}$	0.9867	152.38	0.018
5	SF-G-50 mM $CaCl_2$	$\eta = 0.332\ \gamma^{-0.988}$	0.9957	134.69	0.012

needle with an inner diameter of 200 μm, inserted into the printhead holder of the bioprinting platform, and maintained at 22 ± 1 °C. The constructs were printed at the writing speed of 2 mm/s at 1 bar pressure. After fabrication, bioprinted constructs were kept at RT for cross-linking for 20−30 min and then cultured for 2 days with DMEM high glucose containing 10% FBS and 100 U/mL penicillin/streptomycin. Following fabrication, the constructs were observed using the microscope (Eclipse 90i Nikon, Japan) to evaluate their architecture: the interfilament distance and fiber diameter were measured with a micrometer graticule using 10× magnification. Three measurements per scaffolds/fiber were carried out. Viability, histological, gene and protein expression analyses were carried out to assess the osteogenic potential of constructs.

Osteogenic Differentiation of hMSC-Laden 3D Bioprinted SF-G and SF-G-$CaCl_2$ Constructs. hMSCs laden 3D bioprinted SF-G and SF-G-$CaCl_2$ constructs were transferred to ultra low-attachment 24 well plates to evaluate osteogenic differentiation at 1, 14, and 21 days. To this end, constructs for both SF-G and SF-G-$CaCl_2$ were in part cultured with DMEM high glucose medium, containing 20% FBS and 0.1 μM dexamethasone (Sigma-Aldrich), 100 μM ascorbic acid (Sigma-Aldrich, USA) and 10 nM β-glycerophosphate (Sigma-Aldrich).[24] Moreover, constructs were cultured in control medium, composed of DMEM high glucose with 20% FBS and 25 μM ascorbic acid (Sigma-Aldrich, USA), in order to evaluate the intrinsic osteogenic properties of both constructs at 14 and 21 days. Monolayer cultures of hMSCs were used as positive controls. hMSCs were seeded on 12-well plates and osteogenic differentiation was induced with DMEM containing osteogenic factors (OF) with or without 2.6 mM extracellular $CaCl_2$ as previously reported.[17]

Cell Viability Assessment of hMSC-Laden 3D Bioprinted Constructs. Cell viability of hMSCs laden 3D bioprinted constructs was determined immediately after bioprinting and at the established end-points (day 14 and day 21) by Live and Dead cell viability assay (Thermo Fisher Scientific, USA).[4] Constructs were washed with phosphate buffered saline (PBS) and then incubated with Ethidium homodimer-1 (4 μM) and Calcein AM (2 μM) for 45 min. Labeled cells were then visualized under optical microscope (Nikon, Japan) for evaluating viable (green) and dead (red) cells.

Gene Expression Analysis. hMSCs laden 3D bioprinted SF-G and SF-G-$CaCl_2$ constructs with and without OFs were collected at days 1, 14, and 21 in 1.5 mL tubes with 1 mL of EuroGold RNAPure (EuroClone, Milano) and immediately snap frozen in liquid nitrogen and stored at −80 °C. Total RNA was extracted using a pestle for fragmentation of the constructs to allow better cell lysis according to the manufacturer's protocol. Total RNA was reverse-transcribed into cDNA using first strand cDNA Super Script Vilo cDNA synthesis Kit (Invitrogen, USA) and Real-time PCR was carried out using SYBR Green Master Mix and Rotor gene Q thermocycler (Qiagen, India) using Quantitect primers (Qiagen, India) mentioned in Table 2. The analysis was carried out using the Rotor gene Q software and the relative fold change in the expression levels were calculated using the $2^{-(\Delta\Delta c(t))}$ method[25] with GAPDH as a housekeeping gene. Monolayer hMSCs at day 0 (cultured in the absence of osteogenic factors) were used as comparator or controls to calculate the delta−delta *Ct* relative fold changes.

Table 2. List of Genes Studied for Gene Expression Analysis

sample no.	stage of differentiation	primers
1	housekeeping	GAPDH
2	early-stage markers	RUNX2
3		COL I
4	mid-stage markers	ALP
5		OPN
6		ON
7	mid- to last-stage osteoblast differentiation markers	OCN
8	late osteocytic differentiation markers	PDPN
9		DMP1
10		SOST
11	Wnt signaling specific	β-catenin
12	BMP signaling specific	BMP2
13		BMP4

Histological Analyses for Osteogenic Assessment. Von Kossa staining was performed for both 2D and 3D cell culture conditions, composed of hMSCs with and without OFs, to determine differences in the synthesis of the mineralized matrix.[24] Briefly, constructs were fixed using 10% formaldehyde (Kaltek, Italy) for 15 min at RT, rinsed twice with PBS, and air-dried for Von Kossa staining.

For 3D cultures, hMSCs laden 3D bioprinted SF-G and SF-G-$CaCl_2$ constructs with and without OFs were embedded in OCT and snap-frozen in liquid nitrogen at days 14 and 21. Twelve μm sections were cut, air-dried and stored at −20 °C until their staining. Briefly, for von Kossa staining the slides were normalized at RT, air-dried for 20 min and fixed in 10% formaldehyde (Kaltek, Italy) at RT for 1 h. Then, samples were rehydrated and stained with 5% aqueous silver nitrate (Sigma-Aldrich, USA) solution under ultraviolet light for 30 min, rinsed in deionized water, immersed in 5% sodium thiosulfate solution (Sigma-Aldrich, USA) for 5 min RT. Samples were counterstained with hematoxylin. The quantification of mineralizing processes in hMSCs-laden SF-G and SF-G-$CaCl_2$ constructs was performed by defining a threshold using hue saturation intensity (HSI) system by ImageJ software (NIH, USA). 3D reconstruction of the histological images was obtained using ImageJ 3D plugin (NIH, USA).

Protein Expression Analysis. hMSC-laden 3D bioprinted SF-G and SF-G-$CaCl_2$ constructs were collected in 1.5 mL tubes at day 21 with 100 μL of lysis buffer (Tris-HCl-NaCl-Nonidet P-40-S DS, sodium fluoride (1 mM), sodium orthovanadate (1 mM), phenylmethylsulfonyl fluoride (1 mM), protease inhibitor cocktail (Sigma-Aldrich, Italy, cat. number P83409, diluted 1:200) and immediately snap frozen in liquid nitrogen. Samples were incubated in lysis buffer for 15 min and then centrifuged at 7000 g at 4 °C for 15 min. Supernatants were collected and quantification of the extracted proteins was performed using the Pierce BCA Protein Assay kit (Thermo Fisher Scientific, USA), according to manufacturer instructions and stored at −80 °C. Ten μg protein samples were run on 8% SDS PAGE and the bands of interest from SF-G+OF and SF-G-$CaCl_2$+OF were processed for trypsin digestion as mentioned in

DOI: 10.1021/acsbiomaterials.8b01631
ACS Biomater. Sci. Eng. XXXX, XXX, XXX−XXX

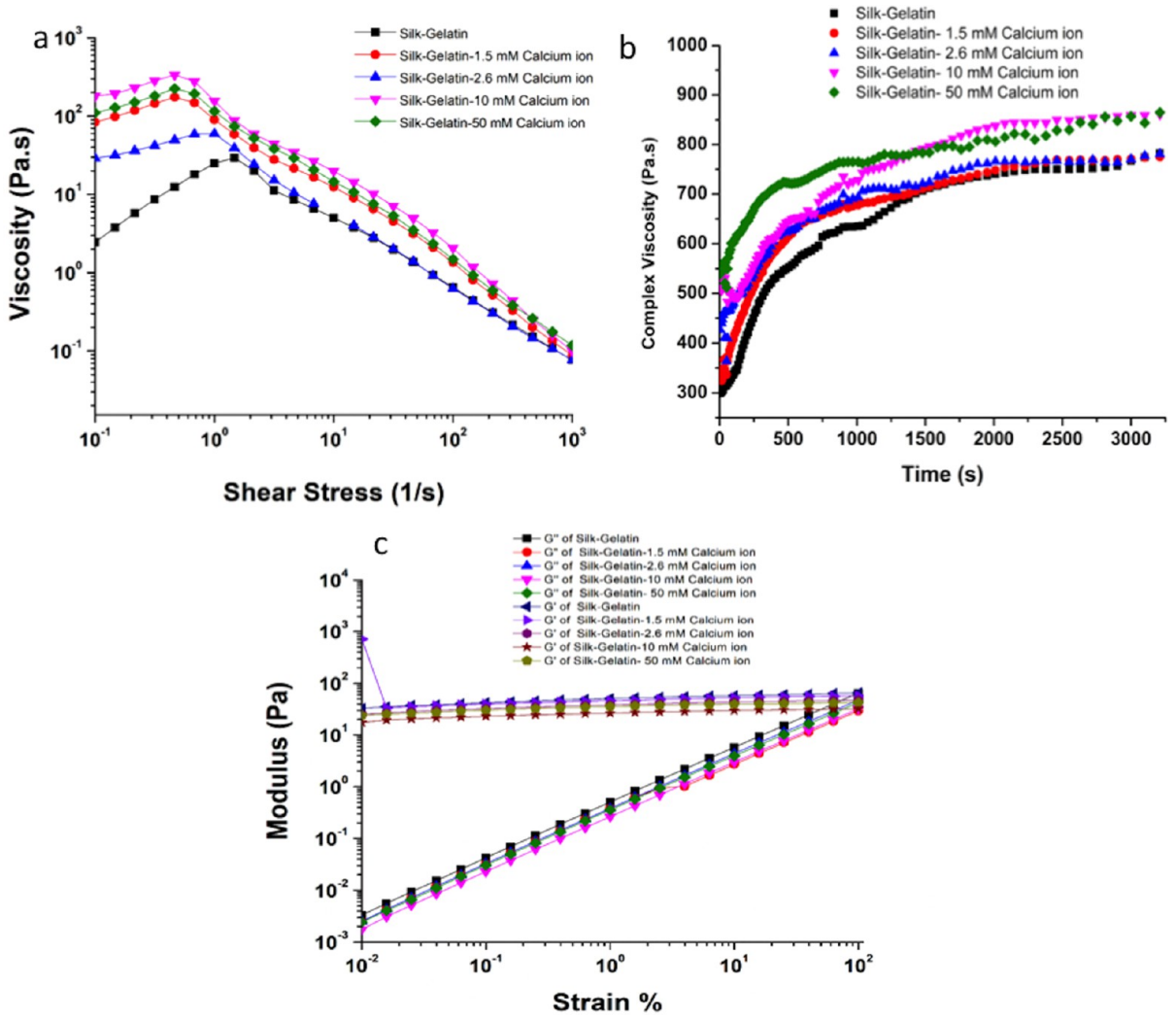

Figure 1. Rheological characterization of the SF-G and SF-G-$CaCl_2$ bioinks formulation. (a) Flow properties of the SF-G without $CaCl_2$, as well as 1.5, 2.6, 10, and 50 mM of $CaCl_2$. (b) Complex viscosity of compositions SF-G- without $CaCl_2$, 1.5, 2.6, 10, and 50 mM of $CaCl_2$ with respect to time, after addition of tyrosinase, at a constant shear rate of 10 s^{-1}. (c) Modulus behavior of the SF-G bioinks- without $CaCl_2$, and 1.5, 2.6, 10. and 50 mM of $CaCl_2$.

our previous study.[25] Matrix assisted laser desorption/ionization-time-of-flight (MALDI-TOF) based mass spectrometric (MS) analysis was performed using Bruker Daltonics Ultraflex MALDI TOF/TOF Mass Spectrometer (Bruker, Germany). Protein identification was performed using MASCOT search engine (Matrix Science) based on MASCOT probability based score using the Swissprot database selecting *Homo sapiens* taxonomy.[26]

Statistical Analyses. Statistical analysis was performed using GraphPad Prism 7 software (San Diego, CA, USA). Normal distribution and homogeneity of variance were evaluated using Shapiro-Wilk test and Levene test, respectively. Data obtained from Von Kossa staining were evaluated with Kruskall-Wallis and Dunn's multiple comparison test. As for gene expression analysis, one-way ANOVA followed by Bonferroni multiple comparison test was used. $P < 0.05$, $P < 0.01$, and $P < 0.001$ were considered significant. Data are represented as the mean ± SD. All the experiments were performed twice using biological triplicates to monitor the performance of each experimental set.

RESULTS AND DISCUSSION

Rheological Optimization of SF-G and SF-G-$CaCl_2$ Blends. All the blends, SF-G, SF-G-1.5 mM $CaCl_2$, SF-G-2.6 mM $CaCl_2$, SF-G-10 mM $CaCl_2$ and SF-G-50 mM $CaCl_2$, showed shear thickening behavior at low shear rates of 0.1 to 1 s^{-1} (Figure 1a). This may be due to the shear-induced β-sheet crystallization or enhanced aggregation and entanglement of the fibroin and gelatin biopolymers. Then, there was sudden shift from shear thickening to shear thinning behavior post 1 s^{-1} until 100 s^{-1}, probably due to rupture of entangled and aggregated morphologies. The transition from shear thinning to shear thickening took place at 0.464 s^{-1} for SF-G-1.5 mM $CaCl_2$, SF-G-10 mM $CaCl_2$, and SF-G-50 mM $CaCl_2$; whereas SF-G and SF-G-2.6 mM $CaCl_2$ shift occurred at 1.5 and 1 s^{-1}, respectively. Above 100 s^{-1}, all the SF-G blends exhibited the same trend of shear thinning, regardless of the composition. Moreover, it was interesting to notice that zero shear viscosity of the SF-G-$CaCl_2$ blends was higher in the order of 100 folds as compared to SF-G blend. This transition from shear thickening to shear thinning behavior can be further described by phenomenological constitutive models, for example, power law equation model for each SF-G-$CaCl_2$ blend (Figure 1a), where η is apparent viscosity, K is flow consistency index, n is power law index, and γ is shear rate.

$$\eta = K\gamma^{n-1} \quad (1)$$

DOI: 10.1021/acsbiomaterials.8b01631
ACS Biomater. Sci. Eng. XXXX, XXX, XXX−XXX

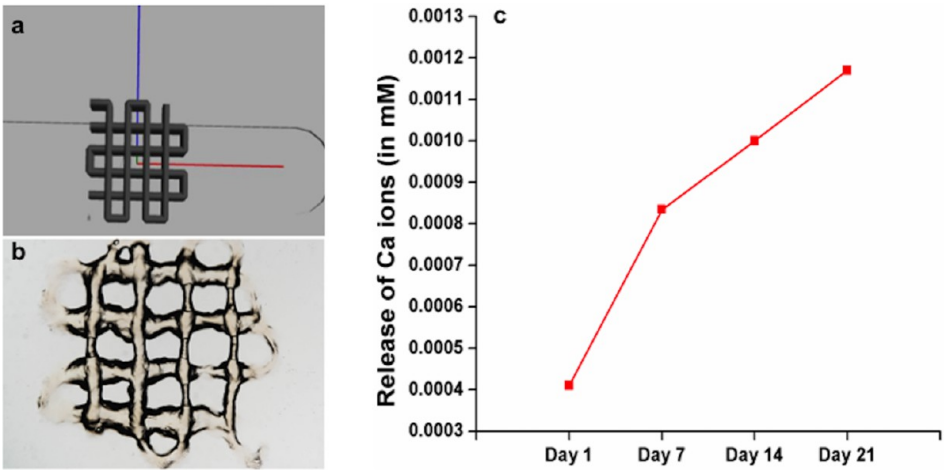

Figure 2. a. CAD image depicting the design parameters of the developed construct. b. Image of 3D bioprinted construct. c. ICP/MS analysis showing the release profile of Ca^{2+} from the SF-G-$CaCl_2$ bioink.

The Ostwald−de Waele power law model was fitted to the average flow curve (Table 1) with all the samples demonstrating a confidence fit of 0.99. All the SF-G compositions with and without $CaCl_2$ exhibited negative slope in the curves. SF-G blends with $CaCl_2$ showed a decreasing trend of n-value with the increase in the calcium content. The flow consistency index, k for SF-G-1.5 mM $CaCl_2$, SF-G-10 mM $CaCl_2$ and SF-G-50 mM $CaCl_2$ is 0.29, 0.332, and 0.357. For SF-G-2.6 mM $CaCl_2$ flow consistency index value is 0.23, closest to 0.116 of SF-G. This indicates that the bioink composition with the 2.6 mM $CaCl_2$ in the SF-G composition displays similarity with only SF-G bioink.

It is important to understand the modulation in flow behavior of the SF-G compositions, with and without $CaCl_2$, postaddition of enzymatic cross-linker, tyrosinase. Hence, the viscosity of the bioink formulations was estimated and correlated with the shear rate at fixed gap over time scales. For all the SF-G-$CaCl_2$ compositions, the viscosity of the bioinks decreased with time (Supplementary Figure 1). To understand how tyrosinase addition would impart gel-like behavior complex viscosity of all the blends, SF-G, SF-G-1.5 mM $CaCl_2$, SF-G-2.6 mM $CaCl_2$, SF-G-10 mM $CaCl_2$ and SF-G-50 mM $CaCl_2$, were estimated with the time-lapse from 0 to 3250 s at a constant shear rate of 10 s^{-1} (Figure 1b). With the increase in the Ca^{2+} concentration in the silk−gelatin bioink, the complex viscosity was increased. The initial complex viscosity of the SF-G-2.6 mM $CaCl_2$ was 427 Pa.s and increased up to 781 Pa.s over the time period of 3250 s. The viscosity of SF-G-2.6 mM $CaCl_2$ after the addition of tyrosinase viscosity increased 113 fold (from 5.63 to 636 Pa.s). SF-G-1.5 mM $CaCl_2$, SF-G-10 mM $CaCl_2$ and SF-G-50 mM $CaCl_2$ showed similar trend. An increase in complex viscosity with time indicated tyrosinase-induced gelation, the extent of which seemed to be dependent on the calcium ion concentration. The shape of the curves were nearly sigmoidal and the initial rate of increase is proportional to the ion concentration, but not at later time points. After the lapse of 2000s, complex viscosity of the bioink composition showed nominal enhancement with time.

$CaCl_2$ induced SF-G blends showed lower storage and loss modulus compared to only SF-G blend (Figure 1c). Storage modulus (G') of all the bioinks were found to be higher than the corresponding loss modulus curves (G'') across the entire frequency range, which is the ideal gelled condition for the biofabrication (Figure 1c). The G'' curves for full range displayed linear increase from 0.01 to 100% strain in log scale. Conversely, storage modulus curve for strain % 0.01 to 100 remains constant for all the blends. At 100 strain %, the values of loss modulus equal storage modulus, which means that beyond 100% strain, the 3D printed scaffold may not exhibit stable structure as energy dissipated will be more than energy stored. Moreover, the low n-value of the power law adds knowledge to our modulus curve, that high storage modulus leads to the slippage between the plate and hydrogel.

Regenerated SF protein solution displays Newtonian behavior,[7] but incorporation of G to the SF protein induced shear thinning behavior of SF-G bioink.[10,12,27] We postulated that this behavior could be due either to the physical formation of cross-linked SF-G semi-interpenetrating network hydrogel[28] or to the presence of opposite charges at physiological pH 7.2−7.4, because the isoelectric points of silk and gelatin are below 7 and above 7, respectively. The gelatin component leaches out during cell culture because of its thermoresponsive nature; however, it is possible to stabilize its structure upon the covalent cross-linking with tyrosinase. In our current study, the addition of $CaCl_2$ in SF-G contributed to increasing its viscosity up to 100 folds at 0.1 s^{-1}. This might be due to the decrease in the gelation time of the SF in the presence of Ca^{2+}. The pH of the SF decreases from 6.5 to 6.8 to 5.6−5.9 in the presence of Ca^{2+}.[29] This shift in isoelectric point of the bioink would contribute to the formation of more stable ionic interactions.[30] Moreover, with reduced repulsion between the neighboring SF chains ease of interactions and higher degree of freedom of movement of protein chains would facilitate self-assembly. Previously,[31] we demonstrated that the optimum concentration of Ca^{2+} ions play an important role in the self-assembly process of SF chains. Ca^{2+} ions stimulate self-assembly and aggregation by interacting with negatively charged amino acid residues, which are predominantly present near the heavy chain end.[29,32] Thus, lower concentrations of Ca^{2+} ions, like 1.5 and 2.6 mM, may promote the β-sheet and distorted β-sheet formation. However, higher concentrations of Ca^{2+} ion, 10 and 50 mM, can sustain predominantly α-helical structural.[33] The covalent bonding between the silk and gelatin molecular chains initiates after the addition of tyrosinase.[10,12] Moreover, during printing, the application of the shear for

DOI: 10.1021/acsbiomaterials.8b01631
ACS Biomater. Sci. Eng. XXXX, XXX, XXX−XXX

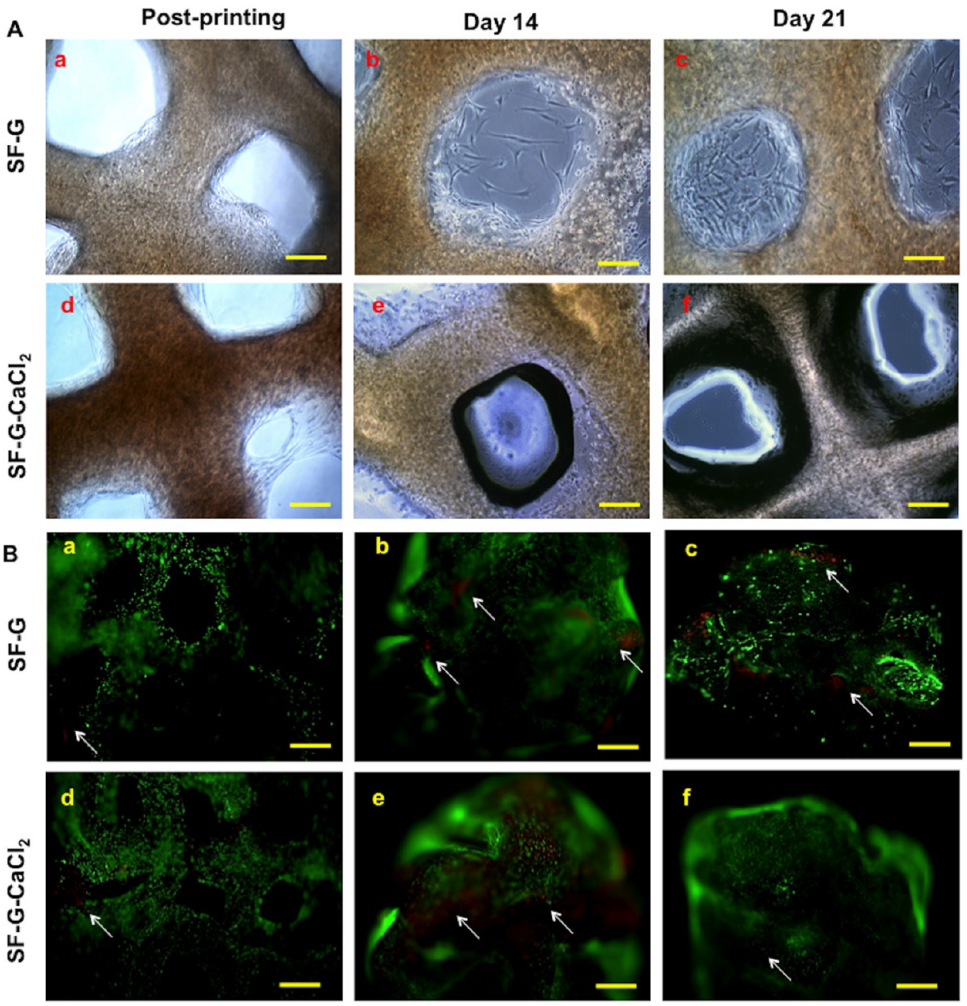

Figure 3. Representative images of (A) cell distribution and (B) live and dead analysis of hMSCs laden SF-G and SF-G-$CaCl_2$ constructs at postprinting and at 14 and 21 days of osteogenic differentiation. (A) (a−c) Photomicrographs from inverted microscopy indicating cell distribution within the SF-G constructs, scale bar: 200 μm. (d−f) Photomicrographs from inverted microscopy indicating cell distribution within the SF-G-$CaCl_2$ constructs, scale bar: 200 μm. (B) (a−c): Photomicrographs from fluorescence microscope of hMSC-laden SF-G constructs, scale bar: 100 μm. (d−f) Photomicrographs from fluorescence microscope of hMSC laden SF-G-$CaCl_2$ constructs, scale bar: 100 μm. Live cells, green staining (FITC); dead cells, red staining (TRITC); white arrows, dead cells.

extrusion leads to shear induced β-crystallization, which would lead to the development of stable 3D-bioprinted SF-G construct. On the basis of the rheological data and the ease of printability, the formulation with SF-G-2.6 mM $CaCl_2$ bioink resulted to be most suitable to perform our studies.

Ion Release Profile of Ca^{2+} Ions. To achieve a controlled in vivo like osteogenic differentiation, there is a strict need of controlling the release of Ca^{2+} from the SF-G matrix. As revealed from the ICP-MS analysis, the calcium ions leached out of the tyrosinase cross-linked SF-G-$CaCl_2$ hydrogel in a sustained manner over the period of 3 weeks (Figure 2c). At different time points, there was the release of 0.4 to 0.5 × 10^{-3} mM of Ca^{2+} in the media suggesting that majority of the 2.6 mM $CaCl_2$ was retained within the SF-G hydrogel construct.

Preparation of Cell-Laden 3D Bioprinted SF-G and SF-G-$CaCl_2$ Constructs. The 3D bioprinted constructs showed open porosity with average fiber diameter of 219 ± 17 μm and pore size (for both SF-G and SG-G-$CaCl_2$ constructs). The constructs were stable after incubation in media throughout the culture period. Microscopic images showed a uniform distribution of the encapsulated cells in both SF-G and SF-G-$CaCl_2$ constructs (Figure 3A) with regular pore distribution and interfilament distance after postprinting step. The preservation of this architecture was observed up to 7 days by inverted light microscopy, whereas swelling occurred afterward. By day 21, the pores of the construct were observed to be closed, likely due to the swelling associated with the SF-G bioink as observed in our previous studies.[4]

Recently, the biological value of extracellular Ca^{2+} as stimulus to foster the mineralization potential of MSCs and osteoblasts[34,35] has been highlighted by several scientists. However, there are a few studies focused on the development of calcium-based composites with SF. Pina et al.[36] developed SF and β-tricalcium phosphate (β-TCP) based freeze-dried porous scaffolds showing osteogenic differentiation potential due to high compressive strength and modulus of the SF and β-TCP scaffolds. Yan et al.[37] reported the development of silk/nanosized calcium phosphate lyophilized porous scaffolds. Xie et al.[38] developed SF and calcium polyphosphate based porous scaffolds that showed improved mechanical properties and lower cellular toxicity over calcium of hydroxyapatite based scaffolds. However, these composite SF-calcium based scaffolds have some limitations, since they were developed using microporous techniques and cells were seeded onto the

DOI: 10.1021/acsbiomaterials.8b01631
ACS Biomater. Sci. Eng. XXXX, XXX, XXX−XXX

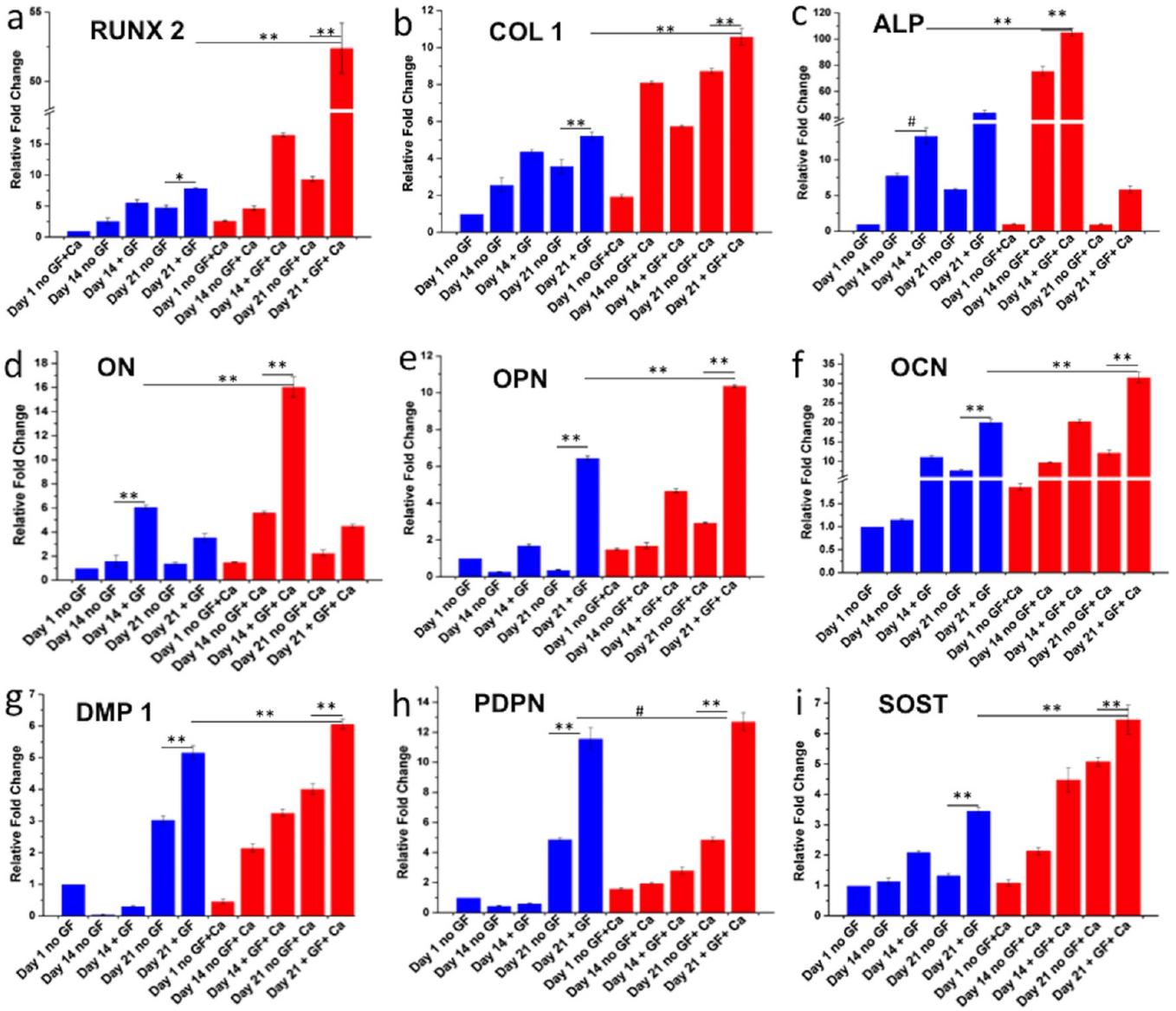

Figure 4. Comparative gene expression analysis for hMSC-laden SF-G and SF-G-$CaCl_2$ constructs for the set of osteogenic differentiation specific genes. # represents significance at $p < 0.05$, * represents significance at $p < 0.01$, and ** significance at $p < 0.001$ wherever applicable.

surface of the scaffolds, offering a putative 2D like microenvironment[39] and thus failing to recapitulate the structural and functional properties of 3D bone microenvironment. These scaffolds could not be used to develop patient-site-specific and defect-site-specific anatomically relevant bone grafts, a limitation that can be overcome by the use of advanced manufacturing techniques such as 3D bioprinting.

Cell Viability Assessment of hMSC-Laden 3D Bioprinted Constructs. Cell viability assessed by live/dead analysis showed the presence of viable cells at all the planned time points in both the experimental groups. Moreover, the cells were observed to be distributed quite evenly in both hMSC-laden 3D bioprinted SF-G and SF-G-$CaCl_2$ constructs (Figure 3B), indicating that both bioprinting process and $CaCl_2$ did not affect their viability.

Role of Extracellular Ca^{2+} in Fostering Osteogenic Differentiation of hMSCs in 3D Bioprinted SF-G-$CaCl_2$ Constructs. To evaluate the differences in the osteogenic differentiation potential between hMSCs cultured in SF-G and in SF-G-$CaCl_2$ constructs with or without OFs, gene expression analysis was performed for a range of osteogenic markers (Figure 4). Both early osteogenic markers, Runt-related transcription factor 2 (RUNX2) (Figure 4a) and type I collagen (COL I) (Figure 4b), were highly expressed in 3D bioprinted SF-G-$CaCl_2$ constructs (7 fold up-regulation of RUNX2 and 2 fold up-regulation of COL I at day 21 as compared to their control without Ca^{2+}) ($p < 0.001$ for COL I and $p < 0.01$ for RUNX2 with and without OFs). The highest expression was found in all samples cultured with OFs compared to the controls without OFs.

The expression of alkaline phosphatase (ALP), a midstage marker, increased during the culture time for the hMSCs laden 3D bioprinted SF-G constructs by reaching the maximum level at day 14 for SF-G-$CaCl_2$ constructs (Figure 4c). Gene expression was higher in all the samples cultured with OFs compared to the controls with no OFs addition. In particular, we observed a 43-fold upregulated expression of ALP in 3D bioprinted SF-G constructs compared to the control at day 1, whereas there was 105-fold upregulated expression in 3D

DOI: 10.1021/acsbiomaterials.8b01631
ACS Biomater. Sci. Eng. XXXX, XXX, XXX−XXX

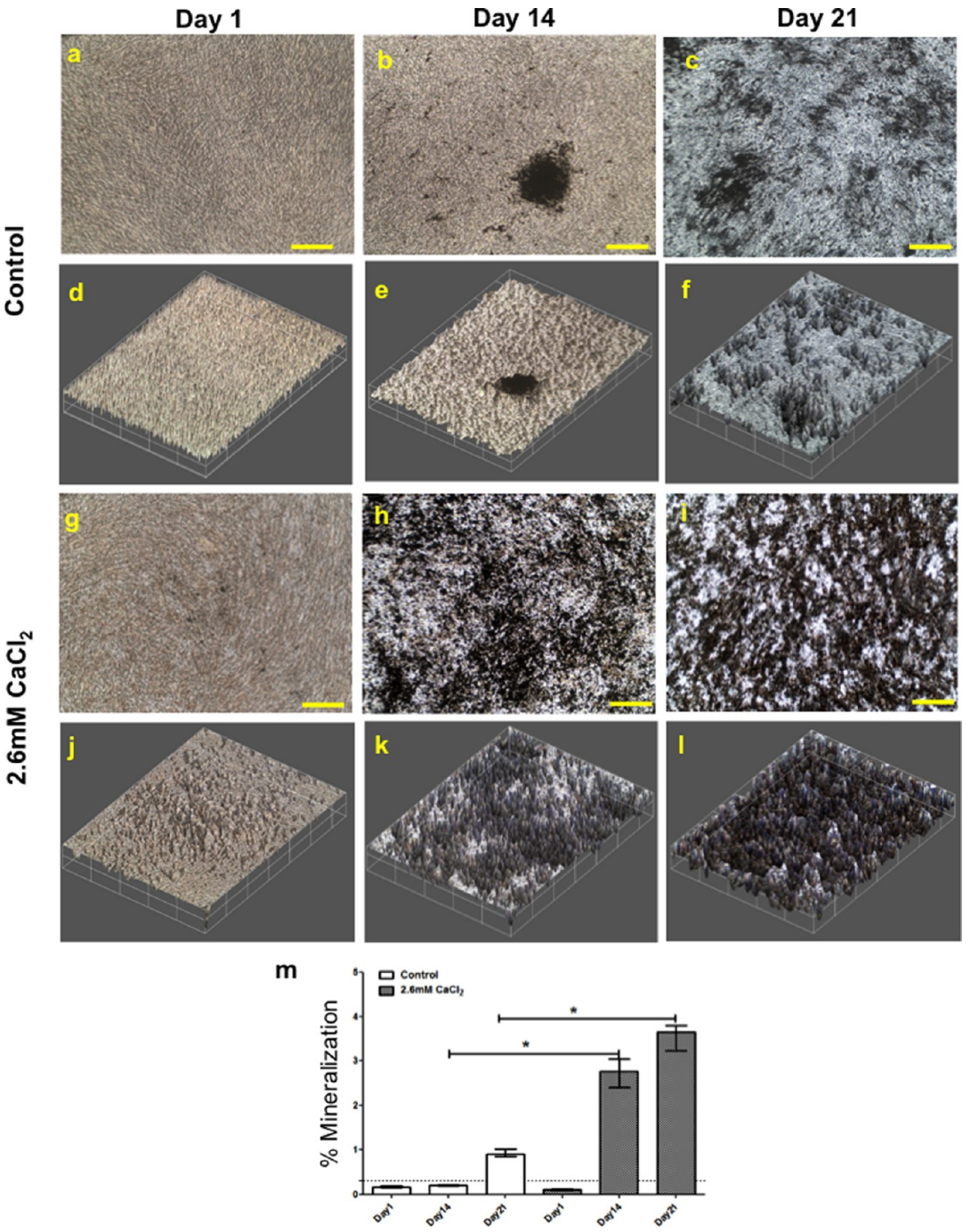

Figure 5. (a–c, g–i) Representative images of Von Kossa staining showing the effect of 2.6 mM $CaCl_2$ on differentiation of hMSCs in monolayer culture. (d–f) Representative 3D reconstructed images of a–c. (j–l) Representative 3D reconstructed images of g–i. Magnification 10×. (m) Histogram showing Von Kossa staining quantification. Dotted line indicates Von Kossa threshold. Data are expressed as mean ± SD. Kruskal–Wallis and Dunn's multiple comparison test were used for statistical analyses (*$p < 0.05$).

bioprinted SF-G-$CaCl_2$ constructs ($p < 0.001$, and $p < 0.05$ for day 14).

The expression of osteonectin (ON) increased until day 14 and declined thereafter for both the hMSC-laden 3D bioprinted SF-G and SF-G-$CaCl_2$ constructs. Its gene expression was higher in SF-G-$CaCl_2$ constructs at all the time points as compared to SF-G constructs (1.5-fold upregulated expression at day 14 where maximum expression was observed in both conditions (data significant at $p < 0.001$) (Figure 4d).

The expression of osteopontin (OPN) increased with the culture time in all the samples with OFs. However, its expression declined for SF-G constructs cultured without OFs (Figure 4e). The expression increased as the culture progressed for all the conditions for SF-G-$CaCl_2$ constructs. Moreover, there was 1.5-fold upregulated expression in the presence of Ca^{2+} in 3D bioprinted SF-G-$CaCl_2$ constructs compared to SF-G constructs at day 21 where the highest up-regulated expression was observed ($p < 0.001$).

The expression of mid to late stage marker osteocalcin (OCN) increased gradually during the culture time for both

DOI: 10.1021/acsbiomaterials.8b01631
ACS Biomater. Sci. Eng. XXXX, XXX, XXX–XXX

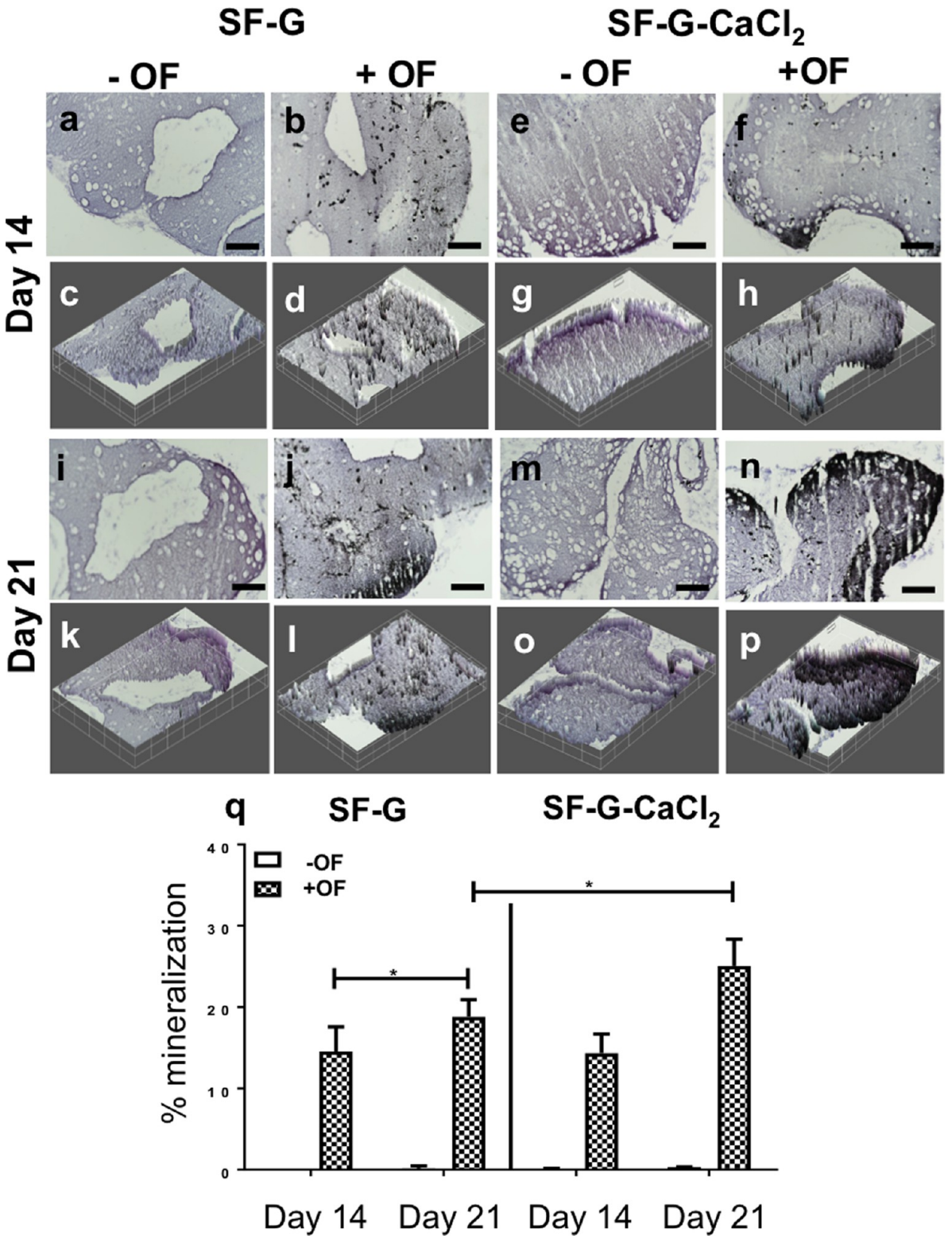

Figure 6. Representative images of Von Kossa staining. (a–d) hMSC-laden SF-G at day 14 (a) without OFs, (b) with OFs, (c) 3D reconstruction of a, (d) 3D reconstruction of b. (e–h) hMSC-laden SF-G-$CaCl_2$ at day 14 (e) without OFs, (f) with OFs, (g) 3D reconstruction of e, (h) 3D reconstruction of f, (i–l) hMSC-laden SF-G at day 14 (i) without OFs, (j) with OFs, (k) 3D reconstruction of i, (l) 3D reconstruction of j. (m–p) hMSC laden SF-G-$CaCl_2$ at day 21 (m) without OFs, (n) with OFs, (o) 3D reconstruction of m, (p) 3D reconstruction of n, scale bar: 100 μm. (q) Histogram showing Von Kossa staining quantification. Data are expressed as mean ± SD. Two-way Anova and multiple comparison test were used for statistical analyses (*$p < 0.05$).

the hMSCs-laden 3D bioprinted SF-G and SF-G-$CaCl_2$ constructs (Figure 4f). The highest expression was found when constructs were cultured with OFs. hMSCs laden 3D bioprinted SF-G-$CaCl_2$ constructs showed higher OCN expression (32 folds at day 21) compared to SF-G constructs (22 folds at day 21) ($p < 0.001$).

DOI: 10.1021/acsbiomaterials.8b01631
ACS Biomater. Sci. Eng. XXXX, XXX, XXX–XXX

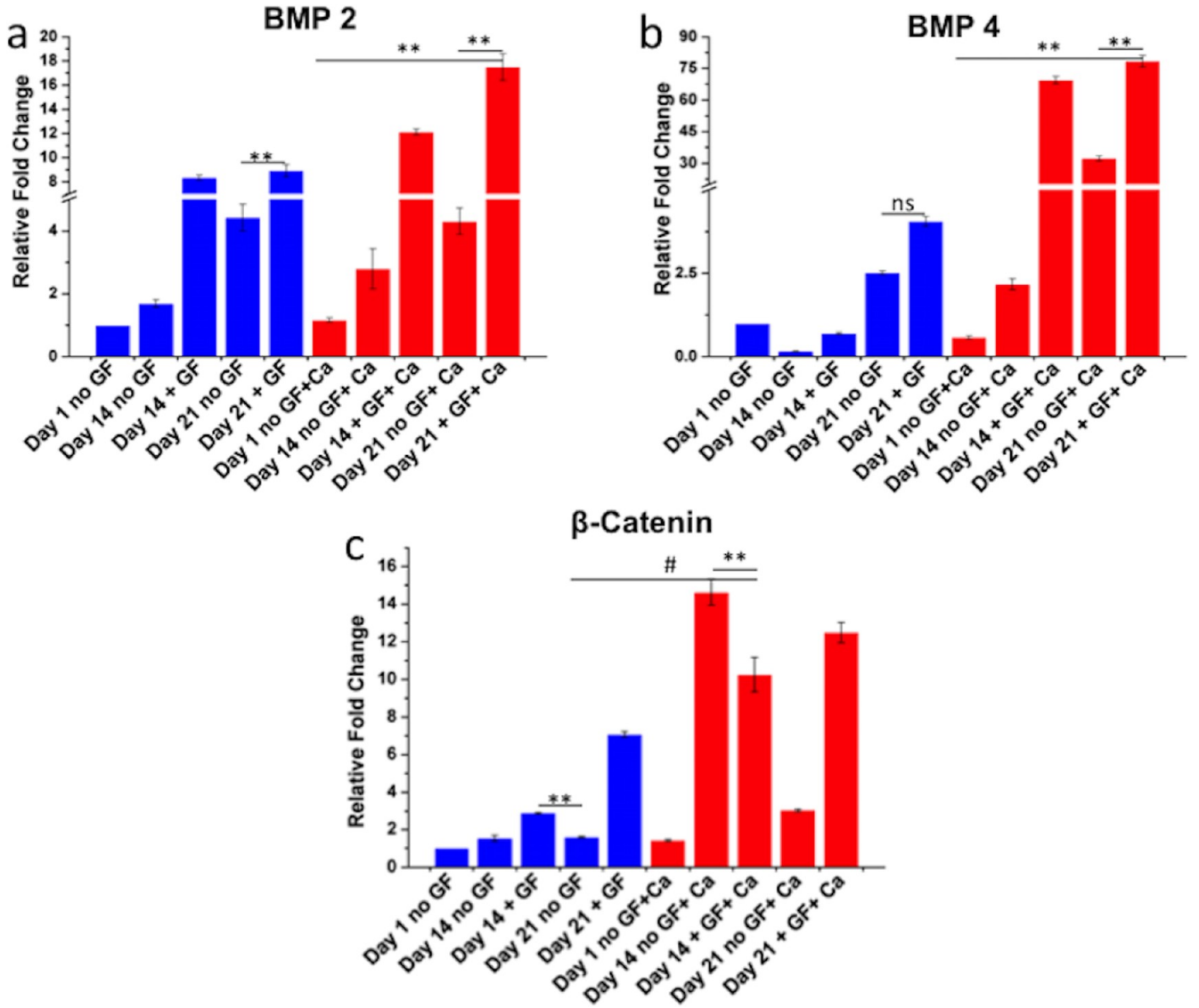

Figure 7. Comparative gene expression analysis for hMSC-laden SF-G and SF-G-$CaCl_2$ constructs for the studied set of osteogenic signaling specific genes. # represents significance at $p < 0.05$, * represents significance at $p < 0.01$, and ** significance at $p < 0.001$ wherever applicable.

The highest expression of late osteocytic markers podoplanin (PDPN), dentin and matrix protein 1 (DMP 1) and sclerostin (SOST) was found at day 21 for both the hMSCs laden SF-G and SF-G-$CaCl_2$ constructs (Figure 4g–i). Moreover, the constructs cultured with OFs showed an upregulated expression compared to the experimental condition without OFs. SF-G-$CaCl_2$ constructs showed upregulated expression of the late osteocytic markers when compared to SF-G constructs (1.2-folds for PDPN and DMP1 and 1.8 folds for SOST ($p < 0.001$ for DMP1 and SOST and $p < 0.05$ for PDPN).

To confirm the induction of osteogenic differentiation using 2.6 mM $CaCl_2$, von Kossa staining was performed in the 2D controls with and without 2.6 mM extracellular $CaCl_2$. Exogenously added 2.6 mM $CaCl_2$ in media significantly induced mineralization from day 14 to day 21 (Figure 5). Compared to the control without Ca^{2+}, cells in Ca^{2+} containing media showed higher mineralization by 9.66 and 4.22 folds at day 14 and 21, respectively ($p < 0.05$) on quantification (Figure 5B). Whereas, the mineralized areas were drastically enhanced in both SF-G and SF-G-$CaCl_2$ constructs (Figure 6). The extent of mineralization increased from day 14 to day 21 and was significantly higher in culture with OFs when compared to the control with no OFs ($p < 0.05$). Hue Saturation Intensity (HSI) based quantitative analysis further confirmed the extent of the mineralization (Figure 6q), where hMSCs-laden 3D bioprinted SF-G-$CaCl_2$ constructs exhibited around 40% higher mineralization at day 21 as compared to SF-G constructs ($p < 0.05$).

Ca^{2+} is one of the main components of the mineral phase that is constantly exchanged with the ECM. Extracellular Ca^{2+} can also upregulate gene and protein expressions related to osteogenesis, including bone morphogenetic protein (BMP)-2, OC and OP.[40−42] Few in vitro studies identified the role of extracellular Ca^{2+} on hMSCs[15,43] by reporting an elevated expression of osteogenic genes in the presence of Ca^{2+}.[15] Correspondingly, in our previous study, we observed increased osteogenic gene expression of osteoblasts in the presence of 2.6 mM extracellular Ca^{2+}[17] by highlighting the role of extracellular calcium in media that positively modulated the intracellular calcium levels. All the above-mentioned studies added valuable insights into the effect of extracellular free Ca^{2+}

DOI: 10.1021/acsbiomaterials.8b01631
ACS Biomater. Sci. Eng. XXXX, XXX, XXX−XXX

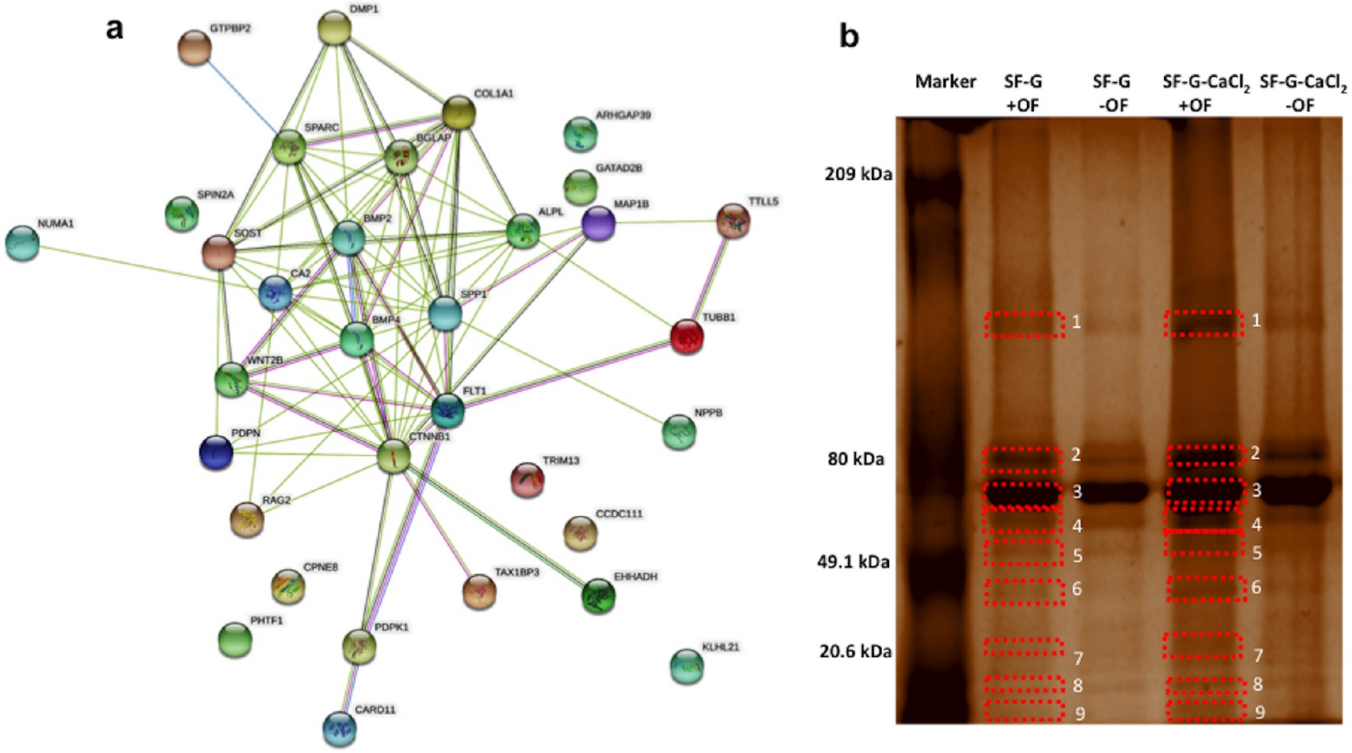

Figure 8. (a) STRING protein−protein interaction for the identified set of proteins. (b) SDS-PAGE showing the bands selected for MALDI-TOF analysis (upregulated in SF-G-$CaCl_2$ constructs as compared to SF-G constructs).

on osteoprogenitors and osteoblasts. However, the shortcomings of these studies are monolayer culture systems and Ca^{2+} being mixed in the media without recapitulating the localized availability of Ca^{2+} in bone tissue. Our previous studies emphasized the inherent properties of SF-G bioink in inducing osteogenic differentiation.[10] For example, the *B. mori* SF owns high mechanical properties as its sequence consists of GAGAGS (glycine (G), alanine (A), and serine (S)) amino acids repeats that contribute to the crystalline nature of silk to form β-sheet structures.[44] Thus, correspondingly, the β-sheet regions present in the SF and the covalent cross-linking induced by tyrosinase probably provided the required stiffness to promote osteogenic differentiation of hMSCs[10] in the 3D bioprinted SF-G and SF-G-$CaCl_2$ constructs. The presence of amorphous anionic bridges between the β-sheets of SF contribute to the mineralization potential of the SF that typically resemble the anionic, noncollagenous regions of collagen type I in the native bone protein[45] providing the nucleation sites for mineral deposition.

Nevertheless, the fact that we observed an increase in the expression of early markers (RUNX2, COLI), mid stage mineralization markers (ALP, OPN, and ON), mid to late stage calcium binding OCN, as well as late stage osteocytic markers PDPN, DMP1 and SOST in the presence of Ca^{2+} is indicative of improved osteogenic potential of hMSCs in the presence of sustained supply of Ca^{2+}. There could be several possible mechanisms related to the interaction of SF and Ca^{2+} that probably contributed to further increase the pro-osteogenic markers and enhanced mineralization. SF contains mineral-binding or hydroxyapatite binding domains primarily composed of acidic residues (glutamate, aspartate, and phosphoserines).[46,47] The availability of these acidic charged groups in the SF provided the overall negative surface charge, thus promoting the binding of positively charged calcium at these residues. We have earlier reported the interaction of Ca^{2+} with the carboxyl (−COOH) containing aspartate and glutamate residues of the SF polypeptide chains thus disrupting the existing hydrophobic interactions and establishment of electrostatic interactions.[31] Another possibility is that Ca^{2+} can bind to other negatively charged groups of SF like, amine (−NH), hydroxyl (−OH), and carbonyl (−C−O) that may provide the nucleation sites for mineral deposition. These interactions probably contribute to the nonspecific binding of Ca^{2+} to SF as observed in our previous study.[31] However, such nonspecific binding is important for maintaining a supply of Ca^{2+} for the cultured cells, which might be difficult in the case of covalent or strong electrostatic interactions. The presence of Ca^{2+} ions lead to induction of more β-sheets in the SF as observed in our previous study,[31] thus possibly providing a stiffer matrix that positively modulated the osteogenic differentiation of hMSCs.

Up-Regulation of Osteogenic Signaling Specific Genes Following the Biological Stimulus with Extracellular Ca^{2+} in the Bioink. The possibility of replicating the signaling pathways of in vivo bone development is essential to identify possible therapeutic strategies for bone repair. To this end, we assessed the gene expression profiles of canonical Wnt pathway specific β-catenin, bone morphogenetic protein (BMP) pathway specific for BMP2 and BMP4. Maximum expression levels of BMP pathway specific for BMP2 and BMP4 were observed at day 21 for both the hMSC-laden SF-G and SF-G-$CaCl_2$ constructs. The expression levels for both these genes were higher in the presence of OFs compared to their absence. BMP2 showed 2-fold upregulated expression (Figure 7), whereas BMP4 showed a massive 26-fold upregulation at day 21 as compared to SF-G constructs ($p <$

DOI: 10.1021/acsbiomaterials.8b01631
ACS Biomater. Sci. Eng. XXXX, XXX, XXX−XXX

Table 3. List of Differentially Expressed Proteins Upregulated in SF-G-$CaCl_2$ and SF-G Constructs

band ID	fold change (SF-G-$CaCl_2$ as compared to SF-G)	mascot score	symbol	name	function	ref
1	1.5	44	TRI13	E3 ubiquitin ligase	regulation of osteoblast survival, proliferation and osteogenic differentiation	58
					interacts with a number of molecules in osteoclasts and is involved with regulation of bone resorption	
2	4.8	62	MAP1B	microtubule associated protein 1MB	cell polarization	71
					autophagy marker along with E3 ubiquitin ligase	
3	2.5	48	P66B	transcriptional repressor p66-beta	upregulated in osteogenic differentiation of hMSCs	59
4	6.5	62	NUMA1	nuclear mitotic apparatus protein 1	organizational features display characteristic patterns during osteogenic differentiation of hMSCs	72
5	2.3	66	RHG39	RhoA-specific GTPase-activating proteins Myo9B	bone growth, phenotype, and cellular activity	64
					decreased patterning of bone osteoclastic podosome, decreasing their motility and resorption capacity	
6	2.1	58	VEGFR1	vascular endothelial growth factor receptor 1	VEGFR1 is involved with cortical bone healing during postnatal stages and is upregulated during bone development	61,63,73,74
					VEGRF1 is also involved in the development of skeletal stem cells, cartilage turnover and bone remodelling	
7	45	53	CPNE8	copine 8	plays a vital role in calcium-regulated intracellular processes for example, calcium-mediated phospholipid-binding	75
8	4.5	56	Wnt-2b	wingless-type-2b	regulates transcription of bone specific genes	68
					interacts with the cell membrane receptors of osteoprogenitors to increase intracellular Ca^{2+}	
9	4.6	43	SPI2A	spindlin2	in vivo functional studies suggest that Spindlin1 activates Wnt/β-catenin signaling	76
10	4.1	46	Pdpk1	3-phosphoinositide-dependent protein kinase 1	involved with prevention of osteoclast apoptosis	77
11	4.2	47	KLH21	Kelch-like protein 21	system development and function	78
12	4.2	49	RAG2	V(D)J recombination-activating protein 2	loss of trabecular bone density and reduced osteoblast number on the bone surface	79
13	4.1	47	CAR11	caspase recruitment domain-containing protein 11	accelerates osteogenesis	80

0.001 for BMP2). The expression levels of β-catenin showed a gradual increase until day 21 of culture in SF-G constructs, whereas the highest expression was observed at day 14 for SF-G-$CaCl_2$ constructs (Figure 7). Moreover, both constructs cultured in the presence of OFs showed an upregulated expression compared to the experimental condition with no OFs ($p < 0.001$ for SF-G; $p < 0.05$ for SF-G-$CaCl_2$). The expression of β-catenin, BMP2, and BMP4 in both SF-G and SF-G-$CaCl_2$ constructs is indicative of involvement of BMP and canonical Wnt/β-catenin signaling pathways in promoting in vitro osteogenic differentiation of hMSCs. We have previously observed the involvement of canonical Wnt/β-catenin signaling in silk-based constructs postulating their possible application in bone tissue engineering.[48] Additionally, in the current study, we deduced the involvement of BMP signaling during in vitro osteogenic differentiation of hMSCs. Nakade et al. reported that a small amount of extracellular Ca^{2+} (0.1−0.4 mM) mixed in media stably upregulates gene expression of BMP2 and BMP4 in osteoblasts cultured in monolayer, but higher concentrations of extracellular Ca^{2+} (1.2−1.4 mM) contribute to delaying the up-regulation of BMP2 and BMP4.[49] ALP activity and osteocalcin secretion were not observed in this study. The marked up-regulation in gene expression of β-catenin, BMP2, and BMP4 in the hMSCs-laden SF-G-$CaCl_2$ constructs confirmed the advantage of extracellular Ca^{2+} tethered in the boink, which was further validated by the KEGG pathway analysis (Figure 8A). Therefore, we can speculate that the up-regulated BMP2 and BMP4 expression in SF-G-$CaCl_2$ constructs could provide a positive response in favoring bone development once implanted in vivo.[48] The probability of crosstalks between Wnt and BMP pathways has been reported by Chen et al.[50] where activation of canonical Wnt/β-catenin signaling was observed in primary calvarial osteoblast cells in the presence of BMP2. Furthermore, the activation of noncanonical Wnt/Ca^{2+} signaling is known in the presence of Ca^{2+}.[51] Correspondingly, in our study, we observed the involvement of Wnt/Ca^{2+} signaling pathway as revealed by the KEGG pathway analysis. Many studies demonstrated that Wnt/Ca^{2+} signaling pathway alone and with Wnt/β-catenin signaling induces osteogenic differentiation, mineralization and ECM deposition by the osteoprogenitors.[48,51,52] The coordinated action of Wnt/Ca^{2+} and Wnt/β-catenin pathways might have led to the translocation of β-catenin into the nucleus of hMSCs encapsulated into SF-G-$CaCl_2$ constructs.[53] KEGG pathway analysis also revealed the involvement of other signaling pathways including parathyroid hormone-dependent signaling pathways (PTH pathway), The forkhead box O (FOXO) pathway and Hippo pathways. Thus, raising the possibility of crosstalk between PTH and Wnt/β-catenin pathway, where PTH might have induced the osteogenic differentiation, mineralization and ECM synthesis of hMSCs in SF-G and SF-G-$CaCl_2$ constructs through activation of Wnt/β-catenin pathway as reported earlier by Romero et al.[54] In vivo extracellular Ca^{2+} exerts its effects on osteoprogenitors by binding to calcium sensing receptors (CaSR). There are many in vitro studies reporting

DOI: 10.1021/acsbiomaterials.8b01631
ACS Biomater. Sci. Eng. XXXX, XXX, XXX−XXX

the confirmed role of CaSR in the induction of proliferation and differentiation of osteoprogenitors.[55] Thus, in our study, the incorporation of extracellular Ca^{2+} might have led to its binding to CaSR on the surface of hMSCs eventually leading to upregulated expression of osteogenic markers in the SF-G-$CaCl_2$ constructs. It is also essential to construe insights about the signaling mechanism how extracellular Ca^{2+} can induce the synthesis of intracellular calcium, or how intracellular Ca^{2+} can get released to initiate matrix mineralization. The prime mechanism could be converged to the involvement of activation of phospholipase C (PLC)-coupled receptors. Inositol-1,4,5-trisphosphate (IP3) is produced in response to binding of extracellular Ca^{2+} to PLC receptors that stimulates the IP3 receptor (IP3R) leading to the release of Ca^{2+} from the endoplasmic reticulum (ER).[56] Similar observations have been made earlier for the release of intracellular Ca^{2+} by murine osteoblasts in an in vitro system by Falsafi et al.[57]

Differential Protein Expression Analysis by hMSCs in the Presence of Extracellular Ca^{2+} in 3D Bioprinted SF-G-$CaCl_2$ Constructs. The differential protein expression profiles of the selected bands of proteins overexpressed in hMSCs laden SF-G-$CaCl_2$ constructs (Bands 1−6 and Bands 8−10) as compared to SF-G constructs and Band 7 specifically present in the SF-G-$CaCl_2$ (Figure 8B) cultured in the presence of OFs were analyzed at day 21 using MALDI-TOF based protein analysis. The list of proteins, as listed in Table 3, includes a number of proteins that positively and negatively modulated the osteogenic differentiation of hMSCs encapsulated in SF-G bioink in the presence of Ca^{2+} (SF-G-$CaCl_2$ bioink). For example, E3 ubiquitin ligase, which was 1.5-fold upregulated in the SF-G-$CaCl_2$ construct compared to SF-G construct, has been known to control osteoblast proliferation, differentiation, and bone resorption through its interaction with osteoclasts.[58] The overexpression of transcriptional repressor p66-beta in SF-G-$CaCl_2$ constructs further validated the observed upregulated osteogenic differentiation in the presence of Ca^{2+}, because it is involved in increasing the expression of octamer-binding transcription factor 4 (Oct4) in hMSCs during osteogenic differentiation.[59] The overexpression of nuclear mitotic apparatus protein 1 (NuMA) provides evidence for improved osteogenic potential of hMSCs in SF-G-$CaCl_2$ constructs because distinctive expression patterns of NuMA protein have been observed during osteogenic differentiation of hMSCs.[60] Moreover, we observed an upregulated expression of vascular endothelial growth factor receptor 1 (VEGFR1) in hMSCs laden SF-G-$CaCl_2$ constructs. It is well-known that VEGFR1 is crucial for in vivo bone formation, bone remodelling and blood vessel development and it is required by osteo-progenitors to decide their osteogenic lineage progression over chondrogenic one.[61] Moreover, the combined action of VEGFR1 and BMP2 could be one of the main reasons for increased osteogenic differentiation and mineralization in the presence of Ca^{2+} in our study, since VEGFR1 enhances BMP2 induced bone formation in vivo.[62] An interesting point to mention here is that the translocation of VEGFR1 from Golgi apparatus to cells plasma membrane is dependent on calcium-regulated process,[63] therefore the upregulation of VEGRF1 in the presence of extracellular Ca^{2+} is quite suggestive of in vivo like calcium-regulated processes. We also observed some proteins that were indicative of in vivo like bone development involved in cytoskeletal arrangement. For instance, a good expression of RhoA-specific GTP-ase-activating proteins (GAPs) Myo9B, involved in modulating the responsiveness of osteoblasts and osteoprogenitors to insulin growth factor-1, was observed in our in vitro system by suggesting its potential in promoting the bone growth.[64]

Furthermore, Halcsik et al. reported an increased expression of microtubule associated proteins 1B (MAP1B) in response to BMP2.[65] Correspondingly, the increased BMP2 gene expression in SF-G-$CaCl_2$ constructs could be the reason for the increase of MAP1B in our study. Additionally, MAP1B along with E3 ubiquitin ligase have been reported to be involved with autophagic response of osteoblasts.[66] Autophagy enhances the osteogenic differentiation potential of hMSCs,[66] several studies have reported the activation of autophagy in response to cytosolic Ca^{2+}.[67] Nevertheless, the most noteworthy observation was the expression of Wnt 2b protein in both hMSCs laden SF-G and SF-G-$CaCl_2$ constructs. Wnt 2b is involved with canonical Wnt/β-catenin mediated induction of osteogenic differentiation in vivo.[68] Therefore, the protein expression of Wnt 2b and gene expression of β-catenin in our 3D bioprinted constructs are indicative of activation of in vivo like canonical Wnt/β-catenin mediated osteogenic differentiation and expression of osteogenic markers. Moreover, the protein expression level of Wnt2b was relatively upregulated in the case of hMSCs-laden SF-G-$CaCl_2$ constructs compared to SF-G constructs by depicting that the involvement of Wnt/β-catenin signaling is more prominent in the presence of Ca^{2+} in the bioink. Another interesting observation in our study was the specific expression of copine 8 in SF-G-$CaCl_2$ constructs. Copine family of proteins have a major role in protein−protein interaction owing to domains that have similarity to integrin binding domain A.[69] Copines contain Ca^{2+} binding domains that respond to increase in the intracellular Ca^{2+},[70] and thus their specific expression corresponds to the presence of intracellular Ca^{2+} in our hMSC-laden SF-G-$CaCl_2$ constructs..

Furthermore, STRING protein−protein interaction network revealed extensive interconnections among the identified proteins (Figure 8A), with 20 hubs identified. The gene ontology analysis showed that the highest connections identified were linked to pathways related to embryonic skeletal joint development, mineral tissue development, ossification, osteoblast differentiation, and bone development. More specifically, KEGG pathway analysis disclosed the list of Wnt/β-catenin signaling pathway, BMP signaling pathway, hippo signaling pathway, FOXO signaling pathway, and thyroid hormone signaling pathway.

Taken together, to the best of our knowledge, this is the first study where the SF-G bioink tethered with Ca^{2+} has been used to develop osteoinductive 3D bioprinted constructs. The newly optimized SF-G-$CaCl_2$ bioink showed optimum rheological properties. We could deduce the first mechanistic insights how the incorporation of Ca^{2+} with the optimized SF-G bioink modulates gene expression and protein production of hMSCs in a preclinical in vitro model as occurs in in vivo bone formation. Our findings offer first basis for the development of unprecedented directed osteogenic differentiation protocols in adult human progenitor cells. Future detailed investigations about the optimization of the bioink composition, printing resolution, the molecular and signaling events of SF-G-$CaCl_2$-based 3D bioprinted constructs and preclinical study for in vivo bone defects models would be mandatory to ascertain its osteogenic potential and its efficacy. Should these analyses improve the bone repair potential of these 3D bioprinted

DOI: 10.1021/acsbiomaterials.8b01631
ACS Biomater. Sci. Eng. XXXX, XXX, XXX−XXX

constructs and applied in a large number of biological samples, there would be the biological premises for the development of patient-specific and defect-site-specific bone implants for clinical applications with proper mechanical properties to ensure its implantation in load-bearing defects.

CONCLUSION

We could develop calcium-conjugated SF-G bioink formulation, whose optimal rheology, sustained calcium release, ionic, as well as covalent cross-linking strategies render it suitable for bioprinting. 3D bioprinted SF-G-$CaCl_2$ constructs enhanced osteogenic potential of hMSCs by (i) upregulating gene expression of osteogenic markers like RUNX2, COL I, ALP, OPN, ON; (ii) upregulating gene expression of osteocytic markers like DMP 1, PDPN, SOST; (iii) upregulating gene expression of β-catenin, BMP2, and BMP4; and (iv) enhancing mineralization processes, compared to the SF-G constructs without calcium. The advantages offered by the inclusion of Ca^{2+} in SF-G bioink was correlated in detail with the mass spectrometry based proteomics analysis. We reported the overexpression of a number of proteins in the presence of Ca^{2+} bound SF-G constructs as compared to only SF-G constructs. This study proposed for the first time a new in vitro model recapitulating a 3D microenvironment based on a gradual calcium release that promoted the osteogenic differentiation of hMSCs at both gene and protein levels with the involvement of in vivo like signaling pathways (canonical Wnt/β-catenin and BMP pathways). To the best of our knowledge, the detailed gene and protein findings from this study provided first insights about the role of silk based matrix with varied stiffness. We further deduced the complex signaling mechanism and cross-talks advantages of combining Ca^{2+}, SF-G bioink and 3D bioprinting technology to improve in vitro osteogenic potential of hMSCs for future bone tissue engineering approaches.

ASSOCIATED CONTENT

Supporting Information

The Supporting Information is available free of charge on the ACS Publications website at DOI: 10.1021/acsbiomaterials.8b01631.

Supplementary data associated with the rheological optimization (PDF)

AUTHOR INFORMATION

Corresponding Authors

*Email: sghosh08@textile.iitd.ac.in (S.G.).
*Email: gina.lisignoli@ior.it (G.L.)

ORCID

Sourabh Ghosh: 0000-0002-1091-9614

Notes

The authors declare no competing financial interest.

ACKNOWLEDGMENTS

This work was jointly funded by Department of Science and Technology, India, and Italian Ministry of Foreign Affairs and International Cooperation.

REFERENCES

(1) Roseti, L.; Parisi, V.; Petretta, M.; Cavallo, C.; Desando, G.; Bartolotti, I.; Grigolo, B. Scaffolds for Bone Tissue Engineering: State of the Art and New Perspectives. *Mater. Sci. Eng., C* **2017**, *78*, 1246−62.

(2) Midha, S.; Murab, S.; Ghosh, S. Osteogenic Signaling on Silk-Based Matrices. *Biomaterials* **2016**, *97*, 133−153.

(3) Melke, J.; Midha, S.; Ghosh, S.; Ito, K.; Hofmann, S. Silk Fibroin as Biomaterial for Bone Tissue Engineering. *Acta Biomater.* **2016**, *31*, 1−16.

(4) Chawla, S.; Kumar, A.; Admane, P.; Bandyopadhyay, A.; Ghosh, S. Elucidating Role of Silk-Gelatin Bioink to Recapitulate Articular Cartilage Differentiation in 3D Bioprinted Constructs. *Bioprinting* **2017**, *7*, 1−13.

(5) Murab, S.; Chameettachal, S.; Bhattacharjee, M.; Das, S.; Kaplan, D. L.; Ghosh, S. Matrix-Embedded Cytokines to Simulate Osteoarthritis-Like Cartilage Microenvironments. *Tissue Eng., Part A* **2013**, *19* (15−16), 1733−53.

(6) Midha, S.; Chawla, S.; Chakraborty, J.; Chameettachal, S.; Ghosh, S. Differential Regulation of Hedgehog and Parathyroid Signaling in Mulberry and Non-Mulberry Silk Fibroin Textile Braids. *ACS Biomater. Sci. Eng.* **2018**, *4* (2), 595−607.

(7) Ghosh, S.; Parker, S. T.; Wang, X.; Kaplan, D. L.; Lewis, J. A. Direct-Write Assembly of Microperiodic Silk Fibroin Scaffolds for Tissue Engineering Applications. *Adv. Funct. Mater.* **2008**, *18* (13), 1883−89.

(8) Fan, H.; Liu, H.; Wang, Y.; Toh, S. L.; Goh, J. C. H. Development of a Silk Cable-Reinforced Gelatin/Silk Fibroin Hybrid Scaffold for Ligament Tissue Engineering. *Cell Transplant.* **2008**, *17* (12), 1389−1401.

(9) Midha, S.; Tripathi, R.; Geng, H.; Lee, P. D.; Ghosh, S. Elucidation of Differential Mineralisation on Native and Regenerated Silk Matrices. *Mater. Sci. Eng., C* **2016**, *68*, 663−674.

(10) Das, S.; Pati, F.; Choi, Y.-J.; Rijal, G.; Shim, J.-H.; Kim, S. W.; Ray, A. R.; Cho, D.-W.; Ghosh, S. Bioprintable, Cell-Laden Silk Fibroin−gelatin Hydrogel Supporting Multilineage Differentiation of Stem Cells for Fabrication of Three-Dimensional Tissue Constructs. *Acta Biomater.* **2015**, *11*, 233−246.

(11) Bhattacharjee, M.; Schultz-Thater, E.; Trella, E.; Miot, S.; Das, S.; Loparic, M.; Ray, A. R.; Martin, I.; Spagnoli, G. C.; Ghosh, S. The Role of 3D Structure and Protein Conformation on the Innate Andadaptive Immune Responses to Silk-Based Biomaterials. *Biomaterials* **2013**, *34* (33), 8161−8171.

(12) Chawla, S.; Sharma, A.; Bandyopadhyay, A.; Ghosh, S. Developmental Biology-Inspired Strategies To Engineer 3D Bioprinted Bone Construct. *ACS Biomater. Sci. Eng.* **2018**, *4* (10), 3545−3560.

(13) Chai, Y. C.; Carlier, A.; Bolander, J.; Roberts, S. J.; Geris, L.; Schrooten, J.; Van Oosterwyck, H.; Luyten, F. P. Current Views on Calcium Phosphate Osteogenicity and the Translation into Effective Bone Regeneration Strategies. *Acta Biomater.* **2012**, *8* (11), 3876−3887.

(14) Aquino-Martínez, R.; Artigas, N.; Gámez, B.; Luis Rosa, J.; Ventura, F.; Cray, J. J. Extracellular Calcium Promotes Bone Formation from Bone Marrow Mesenchymal Stem Cells by Amplifying the Effects of BMP-2 on SMAD Signalling. *PLoS One* **2017**, *12* (5), No. e0178158.

(15) Barradas, A. M. C.; Fernandes, H. A. M.; Groen, N.; Chai, Y. C.; Schrooten, J.; Van de Peppel, J.; Van Leeuwen, J. P. T. M.; Van Blitterswijk, C. A.; De Boer, J. A Calcium-Induced Signaling Cascade Leading to Osteogenic Differentiation of Human Bone Marrow-Derived Mesenchymal Stromal Cells. *Biomaterials* **2012**, *33* (11), 3205−3215.

(16) Dvorak, M. M.; Siddiqua, A.; Ward, D. T.; Carter, D. H.; Dallas, S. L.; Nemeth, E. F.; Riccardi, D. Physiological Changes in Extracellular Calcium Concentration Directly Control Osteoblast Function in the Absence of Calciotropic Hormones. *Proc. Natl. Acad. Sci. U. S. A.* **2004**, *101* (14), 5140−5145.

(17) Gabusi, E.; Manferdini, C.; Grassi, F.; Piacentini, A.; Cattini, L.; Filardo, G.; Lambertini, E.; Piva, R.; Zini, N.; Facchini, A.; et al. Extracellular Calcium Chronically Induced Human Osteoblasts Effects: Specific Modulation of Osteocalcin and Collagen Type XV. *J. Cell. Physiol.* **2012**, *227* (8), 3151−3161.

DOI: 10.1021/acsbiomaterials.8b01631
ACS Biomater. Sci. Eng. XXXX, XXX, XXX−XXX

(18) Fernandez-Yague, M. A.; Abbah, S. A.; McNamara, L.; Zeugolis, D. I.; Pandit, A.; Biggs, M. J. Biomimetic Approaches in Bone Tissue Engineering: Integrating Biological and Physicomechanical Strategies. *Adv. Drug Delivery Rev.* **2015**, *84*, 1−29.
(19) Hak, D. J. The Use of Osteoconductive Bone Graft Substitutes in Orthopaedic Trauma. *Journal of the American Academy of Orthopaedic Surgeons* **2007**, *15* (9), 525−536.
(20) LeGeros, R. Z. Calcium Phosphate-Based Osteoinductive Materials. *Chem. Rev.* **2008**, *108* (11), 4742−53.
(21) Barrère, F.; van Blitterswijk, C. A.; de Groot, K. Bone Regeneration: Molecular and Cellular Interactions with Calcium Phosphate Ceramics. *Int. J. Nanomed.* **2006**, *1* (3), 317−332.
(22) Murab, S.; Samal, J.; Shrivastava, A.; Ray, A. R.; Pandit, A.; Ghosh, S. Glucosamine Loaded Injectable Silk-in-Silk Integrated System Modulate Mechanical Properties in Bovine Ex-Vivo Degenerated Intervertebral Disc Model. *Biomaterials* **2015**, *55*, 64−83.
(23) Nara, S.; Chameettachal, S.; Midha, S.; Singh, H.; Tandon, R.; Mohanty, S.; Ghosh, S. Strategies for Faster Detachment of Corneal Cell Sheet Using Micropatterned Thermoresponsive Matrices. *J. Mater. Chem. B* **2015**, *3* (20), 4155−4169.
(24) Manferdini, C.; Zini, N.; Gabusi, E.; Paolella, F.; Lambertini, E.; Penolazzi, L.; Piva, R.; Lisignoli, G. Immunoelectron Microscopic Localization of Collagen Type XV during Human Mesenchymal Stem Cells Mineralization. *Connect. Tissue Res.* **2018**, *59*, 42−45.
(25) Bhattacharjee, M.; Chawla, S.; Chameettachal, S.; Murab, S.; Bhavesh, N. S.; Ghosh, S. Role of Chondroitin Sulphate Tethered Silk Scaffold in Cartilaginous Disc Tissue Regeneration. *Biomed. Mater.* **2016**, *11* (2), 025014.
(26) Chawla, S.; Ghosh, S. Establishment of in Vitro Model of Corneal Scar Pathophysiology. *J. Cell. Physiol.* **2018**, *233* (5), 3817−3830.
(27) Das, S.; Pati, F.; Chameettachal, S.; Pahwa, S.; Ray, A. R.; Dhara, S.; Ghosh, S. Enhanced Redifferentiation of Chondrocytes on Microperiodic Silk/Gelatin Scaffolds: Toward Tailor-Made Tissue Engineering. *Biomacromolecules* **2013**, *14* (2), 311−21.
(28) Gil, E. S.; Spontak, R. J.; Hudson, S. M. Effect Ofβ-Sheet Crystals on the Thermal and Rheological Behavior of Protein-Based Hydrogels Derived from Gelatin and Silk Fibroin. *Macromol. Biosci.* **2005**, *5* (8), 702−709.
(29) Kim, U. J.; Park, J.; Li, C.; Jin, H. J.; Valluzzi, R.; Kaplan, D. L. Structure and Properties of Silk Hydrogels. *Biomacromolecules* **2004**, *5* (3), 786−92.
(30) Terry, A. E.; Knight, D. P.; Porter, D.; Vollrath, F. PH Induced Changes in the Rheology of Silk Fibroin Solution from the Middle Division of Bombyx Mori Silkworm. *Biomacromolecules* **2004**, *5* (3), 768−772.
(31) Dubey, P.; Murab, S.; Karmakar, S.; Chowdhury, P. K.; Ghosh, S. Modulation of Self-Assembly Process of Fibroin: An Insight for Regulating the Conformation of Silk Biomaterials. *Biomacromolecules* **2015**, *16* (12), 3936−44.
(32) Ochi, A.; Hossain, K. S.; Magoshi, J.; Nemoto, N. Rheology and Dynamic Light Scattering of Silk Fibroin Solution Extracted from the Middle Division of Bombyx Mori Silkworm. *Biomacromolecules* **2002**, *3* (6), 1187−1196.
(33) Zhou, P.; Xie, X.; Knight, D. P.; Zong, X. H.; Deng, F.; Yao, W. H. Effects of PH and Calcium Ions on the Conformational Transitions in Silk Fibroin Using 2D Raman Correlation Spectroscopy And13C Solid-State NMR. *Biochemistry* **2004**, *43* (35), 11302−11311.
(34) Ahlstrom, M.; Pekkinen, M.; Riehle, U.; Lamberg-Allardt, C. Extracellular Calcium Regulates Parathyroid Hormone-Related Peptide Expression in Osteoblasts and Osteoblast Progenitor Cells. *Bone* **2008**, *42* (3), 483−490.
(35) McCullen, S. D.; Zhan, J.; Onorato, M. L.; Bernacki, S. H.; Loboa, E. G. Effect of Varied Ionic Calcium on Human Adipose-Derived Stem Cell Mineralization. *Tissue Eng., Part A* **2010**, *16* (6), 1971−1981.
(36) Pina, S.; Canadas, R. F.; Jiménez, G.; Perán, M.; Marchal, J. A.; Reis, R. L.; Oliveira, J. M. Biofunctional Ionic-Doped Calcium Phosphates: Silk Fibroin Composites for Bone Tissue Engineering Scaffolding. *Cells Tissues Organs* **2017**, *204* (3−4), 150−163.
(37) Yan, L. P.; Silva-Correia, J.; Correia, C.; Caridade, S. G.; Fernandes, E. M.; Sousa, R. A.; Mano, J. F.; Oliveira, J. M.; Oliveira, A. L.; Reis, R. L. Bioactive Macro/Micro Porous Silk Fibroin/Nano-Sized Calcium Phosphate Scaffolds with Potential for Bone-Tissue-Engineering Applications. *Nanomedicine* **2013**, *8* (3), 359−378.
(38) Xie, H.; Gu, Z.; Li, C.; Franco, C.; Wang, J.; Li, L.; Meredith, N.; Ye, Q.; Wan, C. A Novel Bioceramic Scaffold Integrating Silk Fibroin in Calcium Polyphosphate for Bone Tissue-Engineering. *Ceram. Int.* **2016**, *42* (2), 2386−2392.
(39) Chawla, S.; Chameettachal, S.; Ghosh, S. Probing the Role of Scaffold Dimensionality and Media Composition on Matrix Production and Phenotype of Fibroblasts. *Mater. Sci. Eng., C* **2015**, *49*, 588−596.
(40) Dvorak, M. M.; Riccardi, D. Ca2+ as an Extracellular Signal in Bone. *Cell Calcium* **2004**, *35* (3), 249−255.
(41) Tada, H.; Nemoto, E.; Kanaya, S.; Hamaji, N.; Sato, H.; Shimauchi, H. Elevated Extracellular Calcium Increases Expression of Bone Morphogenetic Protein-2 Gene via a Calcium Channel and ERK Pathway in Human Dental Pulp Cells. Biochem. *Biochem. Biophys. Res. Commun.* **2010**, *394* (4), 1093−1097.
(42) Kanaya, S.; Nemoto, E.; Ebe, Y.; Somerman, M. J.; Shimauchi, H. Elevated Extracellular Calcium Increases Fibroblast Growth Factor-2 Gene and Protein Expression Levels via a CAMP/PKA Dependent Pathway in Cementoblasts. *Bone* **2010**, *47* (3), 564−572.
(43) Wagner, A.-S.; Glenske, K.; Wolf, V.; Fietz, D.; Mazurek, S.; Hanke, T.; Moritz, A.; Arnhold, S.; Wenisch, S. Osteogenic Differentiation Capacity of Human Mesenchymal Stromal Cells in Response to Extracellular Calcium with Special Regard to Connexin 43. *Ann. Anat.* **2017**, *209*, 18−24.
(44) Zafar, M. S.; Belton, D. J.; Hanby, B.; Kaplan, D. L.; Perry, C. C. Functional Material Features of Bombyx Mori Silk Light versus Heavy Chain Proteins. *Biomacromolecules* **2015**, *16* (2), 606−14.
(45) Marelli, B.; Ghezzi, C. E.; Alessandrino, A.; Barralet, J. E.; Freddi, G.; Nazhat, S. N. Silk Fibroin Derived Polypeptide-Induced Biomineralization of Collagen. *Biomaterials* **2012**, *33* (1), 102−108.
(46) Addison, W. N.; Miller, S. J.; Ramaswamy, J.; Mansouri, A.; Kohn, D. H.; McKee, M. D. Phosphorylation-Dependent Mineral-Type Specificity for Apatite-Binding Peptide Sequences. *Biomaterials* **2010**, *31* (36), 9422−9430.
(47) Dinjaski, N.; Plowright, R.; Zhou, S.; Belton, D. J.; Perry, C. C.; Kaplan, D. L. Osteoinductive Recombinant Silk Fusion Proteins for Bone Regeneration. *Acta Biomater.* **2017**, *49*, 127−139.
(48) Midha, S.; Chameettachal, S.; Dey, E.; Ghosh, S. Nonmulberry Silk Braids Direct Terminal Osteocytic Differentiation through Activation of Wnt-Signaling. *ACS Biomater. Sci. Eng.* **2017**, *3* (6), 1062−1074.
(49) Nakade, O.; Takahashi, K.; Takuma, T.; Aoki, T.; Kaku, T. Effect of Extracellular Calcium on the Gene Expression of Bone Morphogenetic Protein-2 and −4 of Normal Human Bone Cells. *J. Bone Miner. Metab.* **2001**, *19* (1), 13−19.
(50) Chen, Y.; Whetstone, H. C.; Lin, A. C.; Nadesan, P.; Wei, Q.; Poon, R.; Alman, B. A. Beta-Catenin Signaling Plays a Disparate Role in Different Phases of Fracture Repair: Implications for Therapy to Improve Bone Healing. *PLoS Med.* **2007**, *4* (7), e249.
(51) De, A. Wnt/Ca2+ Signaling Pathway: A Brief Overview. *Acta Biochim. Biophys. Sin.* **2011**, *43* (10), 745−56.
(52) Thrasivoulou, C.; Millar, M.; Ahmed, A. Activation of Intracellular Calcium by Multiple Wnt Ligands and Translocation of β-Catenin into the Nucleus: A Convergent Model of Wnt/Ca2+and Wnt/β-Catenin Pathways. *J. Biol. Chem.* **2013**, *288* (50), 35651−9.
(53) Akhmetshina, A.; Palumbo, K.; Dees, C.; Bergmann, C.; Venalis, P.; Zerr, P.; Horn, A.; Kireva, T.; Beyer, C.; Zwerina, J.; et al. Activation of Canonical Wnt Signalling Is Required for TGF-β-Mediated Fibrosis. *Nat. Commun.* **2012**, *3*, 735.

DOI: 10.1021/acsbiomaterials.8b01631
ACS Biomater. Sci. Eng. XXXX, XXX, XXX−XXX

(54) Romero, G.; Sneddon, W. B.; Yang, Y.; Wheeler, D.; Blair, H. C.; Friedman, P. a. Parathyroid Hormone Receptor Directly Interacts with Dishevelled to Regulate Beta-Catenin Signaling and Osteoclastogenesis. *J. Biol. Chem.* **2010**, *285* (19), 14756−63.
(55) González-Vázquez, A.; Planell, J. A.; Engel, E. Extracellular Calcium and CaSR Drive Osteoinduction in Mesenchymal Stromal Cells. *Acta Biomater.* **2014**, *10* (6), 2824−33.
(56) Berridge, M. J.; Bootman, M. D.; Roderick, H. L. Calcium Signalling: Dynamics, Homeostasis and Remodelling. *Nat. Rev. Mol. Cell Biol.* **2003**, *4* (7), 517−29.
(57) Falsafi, R.; Tatakis, D. N.; Hagel-Bradway, S.; Dziak, R. Effects of Inositol Trisphosphate on Calcium Mobilization in Bone Cells. *Calcif. Tissue Int.* **1991**, *49* (5), 333−339.
(58) Sévère, N.; Dieudonné, F. X.; Marie, P. J. E3 Ubiquitin Ligase-Mediated Regulation of Bone Formation and Tumorigenesis. *Cell Death Dis.* **2013**, *4* (1), e463.
(59) Matic, I.; Antunovic, M.; Brkic, S.; Josipovic, P.; Mihalic, K. C.; Karlak, I.; Ivkovic, A. Expression of OCT-4 and SOX-2 in Bone Marrow-Derived Human Mesenchymal Stem Cells during Osteogenic Differentiation. *Open Access Maced J. Med. Sci.* **2016**, *4* (1), 9−16.
(60) Vega, S. L.; Liu, E.; Patel, P. J.; Kulesa, A. B.; Carlson, A. L.; Becker, M. L.; Moghe, P. V. High-Content Imaging-Based Screening of MicroenvironmentInduced Changes to Stem Cells. *J. Biomol Screen.* **2012**, *17* (9), 1151−1162.
(61) Jacobsen, K. A.; Al-Aql, Z. S.; Wan, C.; Fitch, J. L.; Stapleton, S. N.; Mason, Z. D.; Cole, R. M.; Gilbert, S. R.; Clemens, T. L.; Morgan, E. F.; et al. Bone Formation during Distraction Osteogenesis Is Dependent on Both VEGFR1 and VEGFR2 Signaling. *J. Bone Miner. Res.* **2008**, *23* (5), 596−609.
(62) Peng, H.; Usas, A.; Olshanski, A.; Ho, A. M.; Gearhart, B.; Cooper, G. M.; Huard, J. VEGF Improves, Whereas SFlt1 Inhibits, BMP2-Induced Bone Formation and Bone Healing through Modulation of Angiogenesis. *J. Bone Miner. Res.* **2005**, *20* (11), 2017−27.
(63) Mittar, S.; Ulyatt, C.; Howell, G. J.; Bruns, A. F.; Zachary, I.; Walker, J. H.; Ponnambalam, S. VEGFR1 Receptor Tyrosine Kinase Localization to the Golgi Apparatus Is Calcium-Dependent. Exp. *Exp. Cell Res.* **2009**, *315* (5), 877−89.
(64) McMichael, B. K.; Jeong, Y. H.; Auerbach, J. A.; Han, C. M.; Sedlar, R.; Shettigar, V.; Bähler, M.; Agarwal, S.; Kim, D. G.; Lee, B. S. The RhoGAP Myo9b Promotes Bone Growth by Mediating Osteoblastic Responsiveness to IGF-1. *J. Bone Miner. Res.* **2017**, *32* (10), 2103−2115.
(65) Halcsik, E.; Forni, M. F.; Fujita, A.; Verano-Braga, T.; Jensen, O. N.; Sogayar, M. C. New Insights in Osteogenic Differentiation Revealed by Mass Spectrometric Assessment of Phosphorylated Substrates in Murine Skin Mesenchymal Cells. *BMC Cell Biol.* **2013**, *14*, 47.
(66) Wan, Y.; Zhuo, N.; Li, Y.; Zhao, W.; Jiang, D. Autophagy Promotes Osteogenic Differentiation of Human Bone Marrow Mesenchymal Stem Cell Derived from Osteoporotic Vertebrae. *Biochem. Biophys. Res. Commun.* **2017**, *488* (1), 46−52.
(67) Bootman, M. D.; Chehab, T.; Bultynck, G.; Parys, J. B.; Rietdorf, K. The Regulation of Autophagy by Calcium Signals: Do We Have a Consensus? *Cell Calcium* **2018**, *70*, 32−46.
(68) Ng, J. K.; Kawakami, Y.; Büscher, D.; Raya, A.; Itoh, T.; Koth, C. M.; Rodríguez Esteban, C.; Rodríguez-León, J.; Garrity, D. M.; Fishman, M. C.; et al. The Limb Identity Gene Tbx5 Promotes Limb Initiation by Interacting with Wnt2b and Fgf10. *Development* **2002**, *129* (22), 5161−5170.
(69) Creutz, C. E.; Tomsig, J. L.; Snyder, S. L.; Gautier, M. C.; Skouri, F.; Beisson, J.; Cohen, J. The Copines, a Novel Class of C2 Domain-Containing, Calcium-Dependent, Phospholipid-Binding Proteins Conserved from Paramecium to Humans. *J. Biol. Chem.* **1998**, *273* (3), 1393−1402.
(70) Perestenko, P. V.; Pooler, A. M.; Noorbakhshnia, M.; Gray, A.; Bauccio, C.; Jeffrey McIlhinney, R. A. Copines-1, −2, −3, −6 and −7 Show Different Calcium-Dependent Intracellular Membrane Translocation and Targeting. *FEBS J.* **2010**, *277* (24), 5174−5189.
(71) Bleicher, F.; Couble, M. L.; Buchaille, R.; Farges, J. C.; Magloire, H. New Genes Involved in Odontoblast Differentiation. *Adv. Dent. Res.* **2001**, *15*, 30−3.
(72) Liu, E.; Gordonov, S.; Treiser, M. D.; Moghe, P. V. Parsing the Early Cytoskeletal and Nuclear Organizational Cues That Demarcate Stem Cell Lineages. *Cell Cycle* **2010**, *9* (11), 2108−17.
(73) Maes, C.; Coenegrachts, L.; Stockmans, I.; Daci, E.; Luttun, A.; Petryk, A.; Gopalakrishnan, R.; Moermans, K.; Smets, N.; Verfaillie, C. M.; et al. Placental Growth Factor Mediates Mesenchymal Cell Development, Cartilage Turnover, and Bone Remodeling during Fracture Repair. *J. Clin. Invest.* **2006**, *116* (5), 1230−42.
(74) Uchida, S.; Sakai, A.; Kudo, H.; Otomo, H.; Watanuki, M.; Tanaka, M.; Nagashima, M.; Nakamura, T. Vascular Endothelial Growth Factor Is Expressed along with Its Receptors during the Healing Process of Bone and Bone Marrow after Drill-Hole Injury in Rats. *Bone* **2003**, *32* (5), 491−501.
(75) Jiang, Z.; Jiang, J.; Yang, H.; Wang, Y.; Guo, S. CPNE1 Silencing Inhibits the Proliferation, Invasion and Migration of Human Osteosarcoma Cells. *Oncol. Rep.* **2018**, *39* (2), 643−650.
(76) Su, X.; Zhu, G.; Ding, X.; Lee, S. Y.; Dou, Y.; Zhu, B.; Wu, W.; Li, H. Molecular Basis Underlying Histone H3 Lysine-Arginine Methylation Pattern Readout by Spin/Ssty Repeats of Spindlin1. *Genes Dev.* **2014**, *28* (6), 622−36.
(77) Dobbins, D. E.; Joe, B.; Hashiramoto, A.; Salstrom, J. L.; Dracheva, S.; Ge, L.; Wilder, R. L.; Remmers, E. F. Localization of the Mutation Responsible for Osteopetrosis in the Op Rat to a 1.5-CM Genetic Interval on Rat Chromosome 10: Identification of Positional Candidate Genes by Radiation Hybrid Mapping. *J. Bone Miner. Res.* **2002**, *17* (10), 1761−7.
(78) Hamid, R.; Brandt, S. J. Transforming Growth-Interacting Factor (TGIF) Regulates Proliferation and Differentiation of Human Myeloid Leukemia *Cells. Mol. Oncol.* **2009**, *3* (5−6), 451−63.
(79) Tang, Y.; Wu, X.; Lei, W.; Pang, L.; Wan, C.; Shi, Z.; Zhao, L.; Nagy, T. R.; Peng, X.; Hu, J.; et al. TGF-Beta1-Induced Migration of Bone Mesenchymal Stem Cells Couples Bone Resorption with Formation. *Nat. Med.* **2009**, *15* (7), 757−65.
(80) Sakamoto, T.; Kobayashi, M.; Tada, K.; Shinohara, M.; Io, K.; Nagata, K.; Iwai, F.; Takiuchi, Y.; Arai, Y.; Yamashita, K.; et al. CKIP-1 Is an Intrinsic Negative Regulator of T-Cell Activation through an Interaction with CARMA1. *PLoS One* **2014**, *9* (1), e85762.

DOI: 10.1021/acsbiomaterials.8b01631
ACS Biomater. Sci. Eng. XXXX, XXX, XXX−XXX